Department of Physics and Astronomy
University of Heidelberg

Bachelor Thesis in Physics
submitted by

Stephan Helmrich

born in Neustadt Orla (Germany)

2011

Nuclear Excitation by Electron Capture in Stellar Environments

This Bachelor Thesis has been carried out by Stephan Helmrich at the
Max-Planck-Institute for Nuclear Physics in Heidelberg
under the supervision of
Dr. Adriana Pálffy
and
Prof. Dr. C. H. Keitel

But soft, what light through yonder window breaks?
It is the east, and Juliet is the sun.
Arise, fair sun, and kill the envious moon,
Who is already sick and pale with grief
That thou, her maid, art far more fair than she.[1]

[1]Romeo And Juliet, William Shakespeare Act 2, Scene 2

Abstract

In the resonant process of nuclear excitation by electron capture (NEEC), a free electron recombines into the atomic shell of an ion with the simultaneous excitation of the nucleus. This process is expected to be efficient in populating excited nuclear states in stellar plasmas of high electron density. In this work, we study the possible interplay of NEEC with nuclear excitation by neutron capture as well as associated gamma-decay and neutron emission in the context of nucleosynthesis. Neutron capture followed by beta-decay of the thus formed neutron-rich daughter isotopes constitutes the basic reaction leading to the synthesis of heavy isotopes. For the first time the impact of NEEC taking place prior to the decay of the high-energy state formed by neutron capture is investigated. We show that an additional nuclear excitation of the order of magnitude of 10 keV can cause substantial changes to the net decay rates of the excited nucleus making neutron re-emission predominant. As a consequence, the production of the daughter isotopes would be significantly damped. This first estimate motivates further studies on the impact of NEEC on neutron capture nucleosynthesis.

Zusammenfassung

Kernanregung durch Elektroneneinfang (NEEC) ist die Rekombination eines freien Elektrons unter gleichzeitiger, resonanter Erhöhung des Kernanregungszustandes. Solch ein Prozess stellt einen effektiven Kernanregungsmechanismus in heißen, elektronenreichen Plasmen dar, wie sie in Sonnen auftreten. In dieser Arbeit untersuchen wir mögliche Wechselwirkungen zwischen NEEC und der Kernanregung durch Neutroneneinfang sowie den damit verbundenen Gammazerfall- und Neutronenreemissions-Prozessen des angeregten Zustandes in Verbindung mit Nukleosynthese. Neutroneneinfang, die damit verbundene Produktion eines neuen Tochternuklids und der folgende Betazerfall bilden die grundlegende Reaktionskette der stellaren Nukleosynthese schwerer Isotope. Mit dieser Arbeit wird zum ersten Mal der Einfluss von NEEC, das vor dem Kernzerfall des durch Neutroneneinfang gebildeten, hoch angeregten Tochterkerns stattfindet, untersucht. Wir zeigen, dass eine zusätzliche Kernanregung von wenigen 10 keV eine bedeutende Veränderung der jeweiligen Zerfallsraten verursacht, wodurch Neutronenreemission zum vorherrschenden Zerfallsprozess wird. Als Folge davon wird die Produktion des Tochternuklids stark gehemmt. Diese erste Abschätzung verlangt nach weiterführenden theoretischen Betrachtungen.

Contents

1 Introduction

Our universe exhibits diversity in many aspects, a diversity which often is only absent in the regularity of its constant re-occurrence. Since the old ages this was source and foundation of the striving of man to understand the fabric within nature. This eventually led itself to a diversity in such concepts.

Nature itself is made of an equal variety of elements and their isotopes. A total of 118 elements [Lab11a] are known to man, 90 of which can be found on earth [BBFH57]. Furthermore around 327 isotopes of these elements, either stable or radioactive, occur on earth and well above 3000 of such were already produced by man. Bearing this in mind, it is only natural to wonder how this illustrious abundance of elements was once produced. This process is called *nucleosynthesis*. In particular, it is the curve the number distribution of atomic species takes, which attracts interest. This curve is displayed in Fig. 1.1. Its multi-peaked form, especially the sequence of close double peaks, calls for an elaborate many-process approach as explanation.

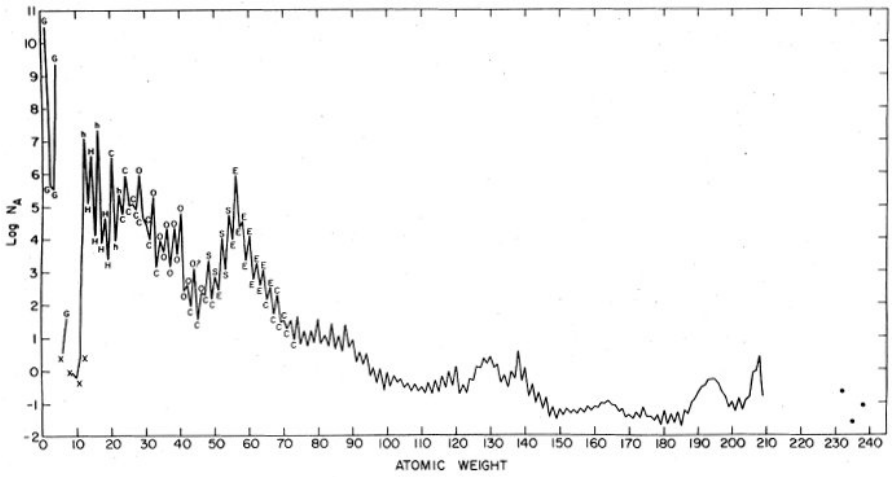

Figure 1.1: Distribution of the abundances N_A as function of the atomic mass A in the solar system. Each datapoint encompasses all isotopes with the same A. Reproduced from Ref. [Tri75].

Already in the 1950s, stars were identified as the centres of nucleosynthesis continuing up to the present time [BBFH57]. Yet nucleosynthesis extends back to earliest times when the mere building blocks of matter were created during *primordial nucleosynthesis*. During these stages of the big bang, all the hydrogen was formed, which serves as the primary input into nucleosynthesis till today.

The constituents of hydrogen, the neutron and the proton, play the primary role in stellar nucleosynthesis. All considered nuclear reactions constitute mainly a redistribution of these nucleons. For elements heavier than ^{56}Fe, nucleosynthesis at large happens by the absorption of free neutrons by nuclei. The thus formed compound nucleus constitutes a new isotope, though in a highly-excited state. This may eventually decay to the ground state by emitting gamma-rays. As this process is driven by neutron absorption, the resulting nuclei often have a surplus of neutrons causing them to be unstable towards beta-decay. Thus, this form of nucleosynthesis can in principle be described as the succession of neutron capture events, followed by the gamma-decay of the excited nuclear state and finally the beta decay of the isotope.

The concept of attributing the abundance of the elements in its variety of aspects to a few basic principles of exchange and interplay of the particles forming every single nuclide was already used with great detail and accuracy by Burbidge et al. in their famous work in 1957 [BBFH57].

One distinguishes two forms of beta-decay, depending on the initial particle being a neutron or a proton. In the neutron converting form, the neutron is spontaneously transformed into a proton inside the nucleus under the emission of an electron and an antineutrino. There only the electron carries a charge, which is used to label this beta-decay form, i.e. this is β^--decay. In the opposite version a proton is converted into a neutron and a positron (the antiparticle of the electron with opposite charge) and a neutrino are emitted. Accordingly, this process is referred to as β^+-decay. Within this picture only these beta-decay processes allow a transition from proton to neutron and vice versa.

From this concept it is already apparent that is is impossible to investigate even the basic nuclear processes without adding two additional species of particles into the pool of particles taken into consideration. These are the photon and the electron. Both contribute in great number density to the stellar plasma and are part of the principal nuclear reactions involved, these being alpha-, beta- and gamma-decay as well as their inverse processes. This list already shows that the minimum particle pool is actually even larger. The great number density of electrons and photons in the stellar environment in connection with their fundamental participation in nuclear reactions makes the consideration of any such process a cornerstone of any nucleosynthesis calculation.

In this work we are mainly concerned with the role of the electron in nucleosynthesis. Besides the already introduced beta-decay, the importance of the electron is underlined by another mode of decay of a nuclear excited state, which mainly occurs for transitions from energetically low states of the nucleus. This is *internal conversion*, where the energy released by the nucleus is, so to say, converted into energy gained by a bound electron. The electron is thereby emitted from the atom. Only recently one attempted to investigate similar effects in the form of the continuum electrons coupling to the internal state of the nucleus. This would constitute the inverse to internal conversion, being called *nuclear excitation by electron capture* (NEEC). This process in principle allows to modify or even control the state occupied by a nucleus through an influx of electrons.

Especially hot dense plasmas like the interior of stars show huge densities of free electrons leading to the expectation of a significant occurrence of NEEC and other processes coupling the atomic shell to nuclear states [GMM10, GMM07, GM04, MMG$^+$10]. This also implies that the reactions leading to nucleosynthesis can possibly be modified by NEEC, thus changing the reaction flow of nucleosynthesis.

The interaction of the stellar plasma with low-lying states of the nucleus is already regarded in the usual nucleosynthesis models by assuming the population of these states to obey thermal equilibrium [KGBA11]. This procedure does not rely on the particular transition mechanisms, so NEEC is already included in this statistical treatment. All the information on the thermal population of low excited states is captured in the so-called *stellar enhancement factor* (SEF) [BBK$^+$00, RT00].

In the common nucleosynthesis model it is assumed that the nucleus decays immediately after formation of the compound state. Only recently it was argued in [BBB$^+$] that the in fact existent life time of the intermediate state suffices to allow the neutron capture to be followed by the absorption of a photon of low energy (less than 1 MeV) prior to the statistical gamma-ray emission. This effect is found to be temperature dependent and to dominate over the direct gamma-decay above a certain temperature. The alternative decay mode to photon emission of the compound state is the re-emission of the previously captured neutron. The branching ratio between these two decay modes is found to be highly sensitive to the energy of the compound state. Therefore, the additional increase of the energy of the nucleus may cause decisive modifications to the probability of the nucleus reaching the ground state of the newly formed isotope. Instead, neutron emission would become dominant. Furthermore it is argued in [BBB$^+$] that this effect is equivalent to a reduction of the neutron separation energy in dependence of the temperature of the environment. In further consequence this leads to a shift of the nucleosynthesis path closer

to the valley of stability.

Up to our knowledge a similar investigation to [BBB$^+$] has never been undertaken for NEEC as an excitation mechanism in the present context. Resonant electron recombination mechanisms like NEEC are believed to be the dominating form of recombination in hot astrophysical plasmas [MB42], where high degrees of ionization and high electron densities arise. Additionally, excitation of the nucleus by coupling to the atomic shell is even more efficient than photoabsorption for nuclear transitions of low energy. These reasons call for the study of the possible impact of NEEC on nucleosynthesis.

In this work we present a first estimate of the possible impact of NEEC occurring on compound nuclei formed by the capture of a slow neutron. Our considerations are founded on the NEEC model developed by Pálffy et al. [PÓ6, PSH06] for NEEC from the ground state, which we will adopt to compound states. For the nuclear excitation energies of compound states, which are of the order of MeV, the nucleus shows no discrete spectrum and measured values of the reduced transition probability entering the calculation of the NEEC transition rates do not exist. Therefore a nuclear level density parametrization obtained from fits to experimental data has to be introduced as well as an approximation of the reduced transition probability. The latter is a rather rough estimate.

The thus calculated numerical values of the NEEC rate for capture into K and L-shell are thereafter embedded into the sequence of neutron capture and decay processes of the compound nucleus. The comparison of the scenarios with and without taking NEEC transitions into account indicates that for a temperature of $k_BT = 30$ keV the probability by which a new isotope is formed decreases by a factor of ten due to NEEC. Thus, NEEC can significantly reduce the formation rate of the consecutive isotope and thus equally reduce the number of neutron-rich isotopes undergoing beta decay. This result, although based on rough estimates, is a cornerstone motivating further theoretical investigations.

This thesis is structured as follows: In chapter 2 we will discuss a basic outline of the processes leading to the nucleosynthesis of heavy elements. This will be followed by a review of the NEEC mechanism and underlying calculations as well as its connection to other atomic and nuclear processes in chapter 3. Thereafter we will combine the presented models in these both chapters to formulate the expressions leading to our estimation of the impact of NEEC. Numerical results obtained for ^{187}Os will be presented and discussed in chapter 5. The work is concluded by a summary and an outline of objectives of further study.

Throughout this work, atomic units with $e = m_e = \hbar = 4\pi\varepsilon_0 = 1$ are used unless specified differently.

2 Stellar Nucleosynthesis

Today there is little doubt that the site of nucleosynthesis are stars and supernovae, which has therefore extended over all ages of the universe since the formation of the first stars and will continue as long as there are such. Although early decisive results were achieved more than 50 years ago, amounting to the first comprehensive review by Burbidge et al. [BBFH57], this field is still an active objective of experimental as well as theoretical research. Especially modern techniques of astronomical observation as well as thorough research campaigns investigating nuclear properties have led to great progress in this field. Notable frontiers are for example the compilation of a distribution of the abundance of the elements or sites of nucleosynthesis and their properties as well as theoretical prediction and modelling [KGBA11, WIP+97].

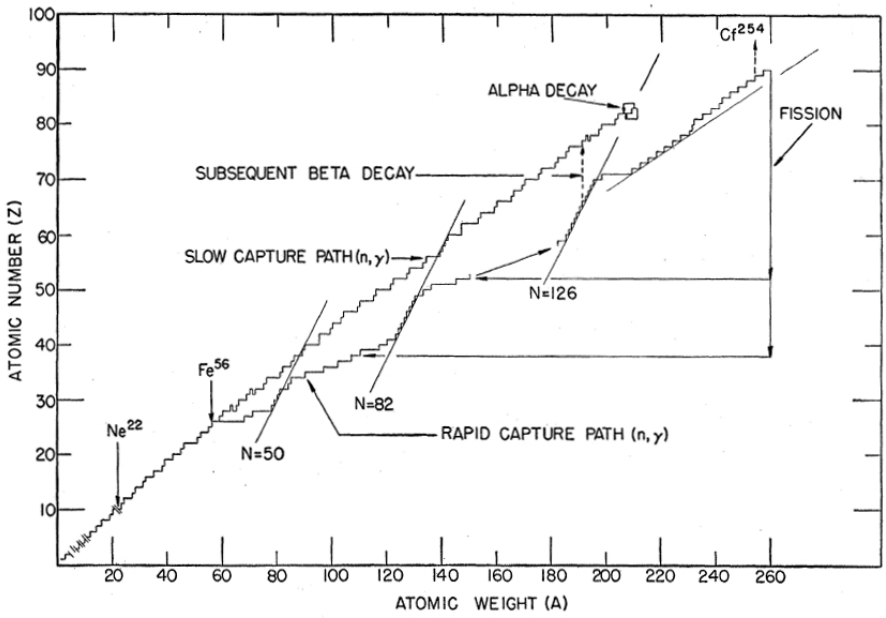

Figure 2.1: The neutron capture paths of the s-process and the r-process. ^{22}Ne and ^{56}Fe are indicated as typical seed nuclei for both mechanisms. The s-process follows the upper line, which is determined by the sequence of stable isotopes and terminated by bismuth. The r-process consists of a rapid sequence of neutron additions and therefore wanders along a path on the neutron-rich side below the line of stability. Waiting points occur here whenever the binding energy of an additional neutron is not sufficient to contain the neutron within the nucleus. These waiting points also mark the so-called neutron drip-off line, which marks the last isotope in a neutron number isobar that can form a compound state with a free neutron. A prominent feature are the staircases, which appear for magic neutron numbers as indicated in the plot. Reproduced from Ref. [BBFH57].

2.1 Principal Nucleosynthesis Processes

The evolution of an isotope undergoes several phases and processes. The need for several independent processes is very well underlined by the shape of the abundance curve in Fig. 1.1, where the series of pronounced peaks can not be explained by nuclear effects alone. The first stage of

chemical evolution of a nucleus is driven by the general tendency of a system to minimize its energy. In a star this results in a drive to increase the average binding energy per nucleon inside a nucleus. Essentially, this happens by fusion, i.e. the formation of a nucleus by merging two lighter nuclei with the same net neutron and proton number. In the context of stellar nucleosynthesis the fusion of helium to other nuclei is dominant. In this way the isotopes will evolve towards ever greater stability and thus ever greater mass, until the maximal binding energy per nucleon is achieved. This process in total encompasses the first stage of nucleosynthesis. It builds towards and terminates at ^{56}Fe with an average binding energy of 8.79 MeV per nucleon, which is therefore the most abundant element of all (compare Fig. 1.1). Further details are not of concern for us, as we will only focus on the astrochemical evolution of heavy elements in this work.

All isotopes heavier than ^{56}Fe are synthesized in processes very different to the one presented so far. The nucleosynthesis of heavy elements results from the addition of neutrons and protons to the nuclei. Especially, these processes themselves are not energetically favourable and happen only in connection to other processes presenting them the necessary input. In this sense the production of all heavy isotopes can be seen as being only a byproduct of the stellar nucleosynthesis of light elements.

Almost all nucleosynthesis turnover for heavy isotopes is achieved by neutron capture processes followed by beta decay. One distinguishes between two regimes of neutron addition nucleosynthesis, depending on whether neutron capture is slow (*s-process*), or rapid (*r-process*) compared to the average beta decay rate of the isotopes on the nucleosynthesis pathway. Beta-decay in its form important here is the process transforming a neutron into a proton inside the nucleus via

$$n \quad \rightarrow \quad p \quad + \quad e^- \quad + \quad \bar{\nu_e}.$$

The electron e^- and antineutrino $\bar{\nu}_e$ are emitted into the continuum.

The s-process is the regime of slow neutron addition compared to the beta decay rate of the nuclei involved. It therefore elaborates along the sequence of stable isotopes. The opposite domain of rapid neutron addition is given by the r-process. Hereby the path of nucleosynthesis leaves the valley of stability towards the neutron rich side. Irrespective of its low nucleosynthesis yields, the *p-process* is noteworthy as well. In this process a proton is captured by the nucleus. However, the p-process is only marginal compared to neutron capture processes as nucleus and proton carry the same sign in charge. The arising repulsive Coulomb force inhibits proton capture at large. Neutrons have a zero charge state and are not subject to any Coulomb barrier.

Nonetheless, all three of these processes are required to successfully describe the abundances of all stable isotopes. One indication for this comes from the shape of the abundance distribution in Fig. 1.1. The double peaks between 120 and 140 as well as between 190 and 210 atomic mass units are an eye-catching feature. These arise because of a nuclear shell effect, where the nucleus can assume a special state of stability whenever a shell is completely filled. These special occupation numbers are also called *magic numbers*, which are 50, 82 and 126. The addition of a new nucleon is then less probable and the abundance of the magic-number nuclei thus builds up. In the course of the s-process, the stable nuclei with such a configuration are directly reached [BBFH57]. Contrary to this, the r-process operates on the neutron rich side of the valley of stability. Thus, the magic number configuration is reached for smaller mass numbers than in the s-process. Once the r-process terminates, the nuclei beta-decay towards the valley of stability and reach it with a quenched neutron number. Therefore, the respective twin peak is shifted towards lower masses. An example illustration of the paths nucleosynthesis may take for neutron addition is given in Fig. 2.1.

Another argument for the necessity to introduce all processes together is given by the positioning of stable nuclei. On the proton as well as the neutron rich side of the main band a number of isolated stable isotopes are situated, as is illustrated in Fig. 2.2. Those nuclei lying on the proton rich side can not be reached through neutron capture, making the alternative addition of protons plausible. On the other side of the valley of stability there are a number of isotopes outside the reach of the s-process, further substantiating the idea of two different neutron capture process

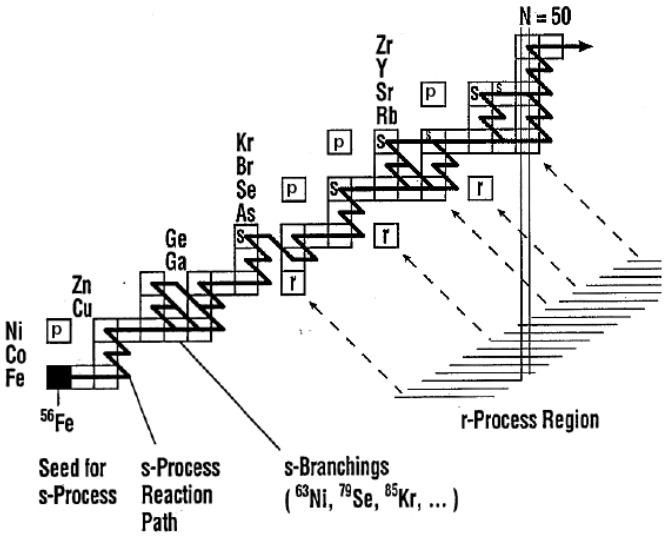

Figure 2.2: Neutron capture processes for the first isotopes starting from ^{56}Fe. Isotopes produced by one process only are marked by the letter of the respective process. Displayed are also important branchings in the s-process path. Reproduced from Ref. [KGBA11]

regimes. Isotopes in such a position shield again the ones lying behind them on the same mass isobar form the r-process. To understand this idea, the reader is again referred to Fig. 2.2.

It is important to note that the scheme outlined here is of course only a simplification of the processes happening in reality in the stellar interior. To divide between s- and r-process is merely an idealization, as both the beta-decay rate and the neutron capture rate can vary considerably between successive isotopes on both paths. The ratios between neutron capture rate, which depends mainly on the abundance of free neutrons itself, and beta-decay rate, which is independent of neutron flux, can thus vary decisively. It is most remarkable that this rather simple picture is still able to produce accurate predictions. Yet this variability of the beta decay rates along the nucleosynthesis path with respect to the neutron capture rates have to be minutely treated, because due to it important variations in the nucleosynthesis path can arise.

2.2 Branching of the Nucleosynthesis Path

A branching point is a stage in nucleosynthesis, where an isotope can be succeeded by different daughter isotopes. This is in a qualitative fashion illustrate in Fig. 2.2. For instance if the neutron capture rate is of the order of the beta decay rate, both events can occur with similar probability, while ruling out one another [BBFH57]. Of course stellar temperature has a crucial impact on the balance of such a branching, as neutron flux and occupation probabilities of lower thermalized levels are altered in accordance to it.

Another mechanism is the occupation of isomeric states. An isomeric state of a nucleus is an excited metastable state, i.e. it is very long-lived. In a number of cases the decay channels open to the isomer differ from the ground state not only in lifetime, but also in type. In this case the branching is fundamental in the sense that its cause are intrinsic properties of the nucleus rather than the external neutron flux. Yet the branching ratio still depends on the stellar environment as the population of the isomeric levels is dependent on the stellar temperature and transitions induced by couplings to the stellar plasma.

In the context of branching points it becomes apparent that the succession of reactions leading to nucleosynthesis very much depends on the stellar environment.

2.3 Stellar Environment Effects

The high temperatures in a stellar medium cause considerable complications for any nucleosynthesis prediction. In essence, high densities of photons as well as free neutrons and electrons together with a high degree of ionization of the atoms arise. This has a variety of consequences, besides allowing nucleosynthesis itself to occur in a notable proportion.

The balance between the arms of a branching point is determined by the stellar environment as was already outlined above. It depends on the probability assigned to neutron capture compared to beta-decay. Both are subject to stellar environment effects.

One rather spectacular consequence of the stellar environment is the enormous enhancement of beta-decay rates with increasing ionization [BFF$^+$96, KGBA11], as beta-decay electrons can then be emitted into a free bound state rather than the continuum. This process is called *bound beta-decay*.

Also the neutron capture rates are subject to couplings to the stellar plasma. When a neutron is captured by a nucleus it forms a so-called *compound state* as an intermediate, highly excited state of several MeV. This state can either decay by re-emitting the neutron, whereby no new isotope is formed, or by the emission of gamma-rays. In the latter the ground state of the thus newly formed daughter isotope. The probability of either decay channel is very dependent on the precise excitation energy of the nucleus. An additional excitation step, even of low energy, lending the nucleus additional energy, can notably modify the probabilities of the two mentioned decay modes.

The high abundance of free particles in the hot, dense environment of stellar plasmas allows a variety of additional excitation mechanisms, e.g. by electrons or photons coupling to the nuclear state. The energy transferred to the nucleus in such interactions is usually of the order of keV, which is low compared to the energy scale of the compound state excitation. An extra nuclear excitation of low energy besides compound state formation can happen before or directly after the capturing of a neutron excites the compound state.

Excitation of the nucleus prior to neutron absorption would result in the compound excitation not happening from the ground state, but from an excited state. State-of-the-art nucleosynthesis calculations include the thermalization of low-lying nuclear states in hot plasmas. Processes leading to the thermal occupation of low-lying states are not addressed specifically, but in a process-independent statistical approach, in which also NEEC is already implicitly accounted for. In this procedure neutron capture on low-lying nuclear states including the ground state is incorporated into the calculation of a theoretical of the neutron capture cross section, averaged over the spectrum of free neutrons. This cross section is called *Maxwellian-averaged cross section*. Its ration with the measured neutron capture cross section under laboratory conditions is the *stellar enhancement factor*, which signifies the enhancement neutron capture is expected to have under stellar conditions compared to the laboratory.

In the alternative scenario a low-energy excitation is built on an excited nuclear compound state. A further excitation of the compound nucleus before its decay is favoured by an increasing nuclear level density with increasing excitation energy. Already a small additional excitation of the high-energy state of the compound nucleus can lead to a substantial increase in nuclear level density, thus rendering excitation prior to spontaneous decay possible.

This idea was investigated for photon excitation by Bernstein et al. in Ref. [BBB$^+$]. In our work we introduce nuclear excitation by electron capture as an additional excitation mechanism. Therein, an electron is captured into a bound state of the atom, whereby the released energy is resonantly transferred to the nucleus, which in consequence of this is excited. It was already shown by Pálffy [PEK07] that this excitation mode is most efficient for low energies of the impinging electron. In this regime it can even be a more effective excitation mode than nuclear excitation by photon absorption.

As was also discussed in [PEK07], NEEC is a not negligible mechanism allowing the depletion of the occupation of isomeric states via the excitation to higher excited states; similar results were found in [GMM07].

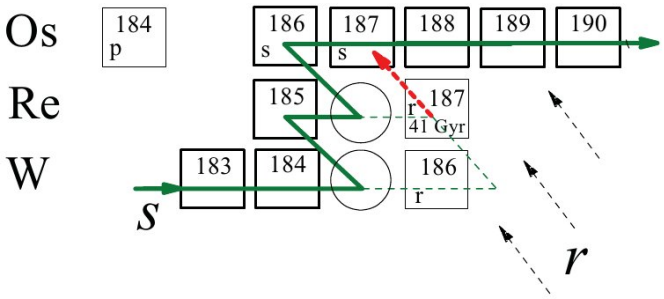

Figure 2.3: The reaction paths contributing to the Re/Os clock. The path of the s-process is marked in green, with the main path drawn in a bold line, while side branches are shown as a dashed line. The isotopes causing such a branching are shown as circles. The reaction flow of r-process synthesis is marked by dashed arrows. The radiogenic production of ^{187}Os is marked by a red arrow. Isotopes being produced by one reaction only sport the letter associated to the respective process. Reproduced from Ref. [MFM$^+$10].

2.4 The Re/Os-Clock

There are stations in the path of nucleosynthesis of special interest, because by chance of a peculiar assembly of isotopes with specific decay properties further knowledge may be derived about the setting of nucleosynthesis. Prominent examples for this are cosmochronometers and cosmothermometers. In the past, a number of cases has been proposed and succeedingly investigated. One of the most promising and thoroughly investigated one is the Re/Os clock. It was first proposed by Clayton [Cla64]. In the following we will as well focus on this case and investigate a choice of its isotopes.

The basic reaction flow is displayed in Fig. 2.3 and reveals the concept of this galactic clock. The isotope which serves as the timer is ^{187}Re with a beta decay half-life of 41 Gyr. This is the same order as the expected age of the universe and therefore a suitable candidate for estimating this time.

Furthermore, ^{186}W and ^{187}Re shield the osmium isotopes ^{186}Os and ^{187}Os from the r-process, so that they are produced in the s-process only, except form radiogenic contributions (i.e. contributions arising due to the decay of other isotopes, namely ^{187}Re here). This simplifies calculations considerably and reduces the dependency on the number of involved isotopes considerably. A thorough analysis has to account for the branchings of ^{185}W and ^{186}Re, though. The alteration of these branchings by including NEEC in the network of considered reactions would form one object of study for us. If the s-process contribution to the ^{187}Re abundance could be safely neglected, the measured abundance would result from r-process only. This would allow a rather straightforward determination of the galactic age from r-process nucleosynthesis models [FMM$^+$10].

The information on the age of the universe is in either way captured by the radiogenic abundance $N_c(^{187}\mathrm{Os})$, i.e. the proportion synthesized by beta-decay of ^{187}Re. It can be derived by subtraction of the s-process abundance from the total one,

$$N_c(^{187}\mathrm{Os}) = N_{\mathrm{total}}(^{187}\mathrm{Os}) - N_s(^{187}\mathrm{Os}). \tag{2.1}$$

N_{total} can be taken from measurements. Thus far the s-process abundance of ^{187}Os was not established. This value can be obtained by considering the production of ^{187}Os in s-process nucleosynthesis from its direct predecessor ^{186}Os and the production to the seccessing isotope [FMM$^+$10, BBFH57]. This requires the investigation of neutron capture properties of both idotopes. This underlines the importance of the study of the neutron capture cross sections of these two isotopes.

Unfortunately one major problem within this framework of the Re/Os clock is the beta-lifetime of ^{187}Re itself. This isotope is subject to a very short bound beta-decay half-life, once the isotope attains a very high degree of ionization. In the case of fully ionized $^{187}\mathrm{Re}^{75^+}$, the half-life is known

to decrease by full 9 orders of magnitude [BFF$^+$96]. In total, the effect introduces an uncertainty of $2 - 4$Gyr to the age estimate [Tak98]. Other problems concern the theoretical prediction of the afore mentioned $\langle\sigma\rangle$ cross section values under stellar conditions [ATY84]. Furthermore the mentioned s-process contribution to ^{187}Re has to be addressed [SUM$^+$05, KJBR91].

Estimates derived by this method compete with those of other, completely independent approaches, such as the Hubble age, globular cluster age or cosmic microwave background age.

Within the Re/Os clock the precise knowledge of the neutron capture cross sections of the isotopes ^{186}Os, ^{187}Os ^{185}W and ^{186}Re was shown to be of crucial importance. Hence, we chose one of these isotopes, namely ^{187}Os, as an example for determining the impact of nuclear excitation by electron capture on the net neutron capture process.

3 Formalism of NEEC

3.1 Electron Recombination Mechanisms

The hot dense solar plasma constituting the environment of nucleosynthesis features a high density of free electrons. This great abundance occurs due to the high ionization degree of the atoms in a stellar plasma. Free electrons can in turn interact with the remaining ions leading to a variety of processes, most importantly electron scattering and electron capture into a previously unoccupied bound state. If the latter results in the emission of a photon which carries the excess energy, this is called *photo recombination* (PR). This general term is used without regard to the underlying recombination mechanism.

A subdivision is possible according to whether the underlying recombination is resonant or not. In the direct, non-resonant reaction path the photon is emitted directly upon binding of the electron. This *radiative recombination* (RR) of the electron presents a major background contribution for measurement and analysis of electron recombination mechanisms and is also a very important electron recombination process in astrophysical plasmas.

On the contrary the resonant channel occurs as displayed in Fig. 3.1 if in a first step another, already bound electron is simultaneously excited. Afterwards this excited state may decay by photon emission. Note that this process is only possible if the transition energies of both electrons involved match. To this resonant channel of PR one refers as *dielectronic recombination* (DR). The first step taken alone is accordingly called *dielectronic capture* (DC); the corresponding inverse process to DC is Auger recombination. There the excited bound electron decays back to an unoccupied lower level while simultaneously ejecting a second electron. Dielectronic recombination is regarded as the dominant recombination mechanism in the high temperature environment of the stellar interior.

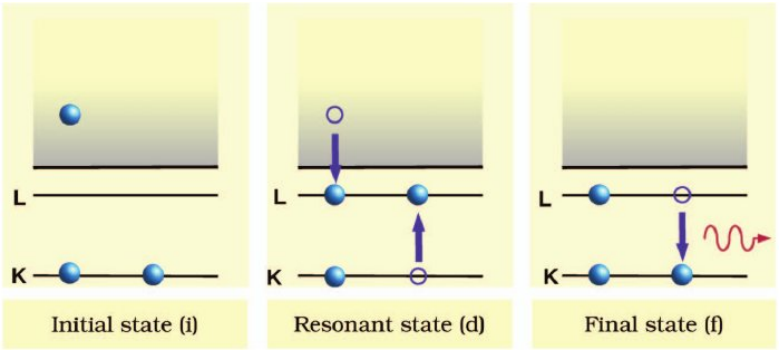

Figure 3.1: Dielectronic recombination. A free electron is captured into the L shell of a He-like atom. Resonantly, a K shell electron is excited to the L shell. This recombination is followed by the radiative decay of the excited electron. With the involved shells specified as such this process is also called KLL-DR process. Reproduced from Ref. [Pá10].

This kind of mechanism is of interest for nuclear physics if instead of the second electron, the nucleus is excited, i.e. the initial electron is captured into an open atomic level, while its energy is simultaneously transferred to the nucleus. This is *nuclear excitation by electron capture*, short NEEC. It is a photo recombination process if in a consecutive step the excited nucleus decays by emitting a photon. An illustration of NEEC followed by photon emission can be found in Fig. 3.2 for the electron being captured into the lowest free atomic state. Otherwise the decay

of the electron to the lowest state could be included as an additional step. The reverse of NEEC is *internal conversion* (IC), wherein a nuclear excited state is deexcited by resonantly exiting a bound electron into the continuum. In fact this can be another possible decay channel of the final excited nuclear state of NEEC. NEEC followed by IC constitutes a form of resonant electron scattering.

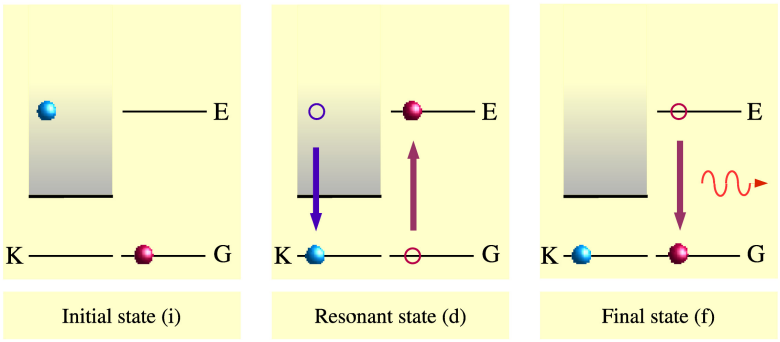

Figure 3.2: Nuclear excitation by electron capture. Note the close similarity to Fig. 3.1, where the nuclear part is only replaced by an additional bound eletron state. Reproduced from Ref. [PÓ6].

Mainly because RR poses such a large background, the observation of NEEC did not succeed so far [Dau06, gsi89], although the process was first proposed already in 1976 by Goldanskii and Namiot [GN76]. Yet the reverse process, IC, is well established as a decay channel of excited nuclei. Furthermore, the process *nuclear excitation by electron transition* (NEET), which differs from NEEC only in the initial electron state being a bound state rather than a continuum one, was already observed [KYS$^+$00]. Additionally, the inverse of NEET, called *bound internal conversion* (BIC), was also already observed in an experiment [CHA$^+$00]. Taking these findings together, there is no doubt about the excistence of NEEC; for measurement proposals we refer to [PEK07, PHK$^+$08, PÓ6].

In this work we will use the comprehensive approach developed by Pálffy [PÓ6] to calculate the rate of NEEC. In the work of Pálffy the cross section of the full two-step process encompassing excitation of the nucleus by NEEC and its consecutive deexcitation mechanism was treated. This cross section is found to be proportional to the rates of both steps, thus yielding the desired NEEC rate. This rate will be taken from [PÓ6] and invoked in chapter 4 into the network of rates leading to the formation of a new isotope by neutron capture.

In the remaining parts of this chapter we will review the approach of Pálffy and outline important steps in the consideration.

3.2 Decomposition of the Configuration Space and the System's Total Hamiltonian

First of all the considered process of NEEC followed by photon emission is divided in its steps as discussed above and illustrated in Fig. 3.2. For every step the quantum state of the entire system comprising electron, photon and nucleus is denoted by the direct product of the individual state vectors:

$$|\,\Psi\rangle = |\,\text{nucleus}\rangle \otimes |\,\text{electron}\rangle \otimes |\,\text{photon}\rangle = |\,\text{nucleus, electron, photon}\rangle. \tag{3.1}$$

The initial state (i) is defined by an electron in a continuum state, while the nucleus is in a state of choice depending on the process under consideration and no photon exists in the photon field:

$$|\,\Psi_i\rangle = |\,N_i I_i M_i\rangle \otimes |\,\vec{p} m_s\rangle \otimes |\,0\rangle. \tag{3.2}$$

Here N is used to express the nuclear state, of which I_i is the nuclear angular momentum and M_i its projection. Furthermore, $\vec{p}$ is the asymptotic momentum of the electron with spin state m_s. An intermediate state (d) is introduced to represent the configuration of captured electron and thereby excited nucleus,

$$\mid \Psi_d\rangle = \mid N_d I_d M_d\rangle \otimes \mid n_d \kappa_d m_d\rangle \otimes \mid 0\rangle, \tag{3.3}$$

with n_d, κ_d and m_d being the principal angular momentum quantum number, the Dirac angular momentum quantum number and the magnetic quantum number, respectively, of the now bound electron. The final state (f) is then formed upon deexcitation of the nucleus by emission of a photon:

$$\mid \Psi_f\rangle = \mid N_f I_f M_f\rangle \otimes \mid n_d \kappa_d m_d\rangle \otimes \mid \vec{k}\varsigma\rangle, \tag{3.4}$$

with

$$\mid \vec{k}\varsigma\rangle = a^\dagger_{\vec{k}\varsigma} \mid 0\rangle. \tag{3.5}$$

Here $\vec{k}$ and $\varsigma = 1,\ 2$ are the respective wave vector of the photon and its transversal polarization. Eq. (3.5) employs the creation operator $a^\dagger_{\vec{k}\varsigma}$ of a continuum photon. Applying this operator to any photon state will raise the number of photons in the mode of the field characterized by $\vec{k}$ and ς by one. In the following, we will denote nuclear quantum numbers by capital letters and the respective electron angular momenta by lower-case letters.

The method as it was formulated in [PÓ6, PSH06] relies on projection operators mapping into the subspaces spanned by the states as introduced above. The initial state is characterized by the energy ε of the free incoming electron. With p symbolizing the remaining, discrete quantum numbers, the projection operator onto the space of initial states is given by

$$P = \int \mathrm{d}\varepsilon \sum_p |p\varepsilon\rangle\langle p\varepsilon| \,. \tag{3.6}$$

Employing another cumulative index for the quantum numbers of the bound electron and the nucleus, the projection operator of all intermediate states can be written as

$$Q = \sum_q |q\rangle\langle q| \tag{3.7}$$

and similarly for all final states:

$$R = \sum_q \sum_{\vec{k}\varsigma} a^\dagger_{\vec{k}\varsigma} \, |q\rangle\langle q| \, a_{\vec{k}\varsigma}. \tag{3.8}$$

Following [PÓ6] we postulate that the relation

$$P + Q + R = 1 \tag{3.9}$$

holds for the projection operators. Thereby the total configuration space of the process was separated into subspaces defined by the projection operators given above. This formalism is in general called *Feshbach projection operator formalism.*

The total Hamilton operator H can be separated into an interaction Hamilton operator H_I and a state Hamilton operator H_0 via

$$H = H_0 + H_I \tag{3.10}$$

with

$$H_0 = PHP + QHQ + RHR \tag{3.11}$$

and

$$H_I = PHQ + PHR + QHR + QHP + RHP + RHQ. \tag{3.12}$$

The interactions described in the last equation amount to mappings from one subspace of configurations into another, thus defining all possible transitions. The type of interaction is specified as follows:

$$RH_IP = H_{er}; \qquad PH_IR = H_{er} \tag{3.13a}$$
$$QH_IP = H_{en}; \qquad PH_IQ = H_{en} \tag{3.13b}$$
$$QH_IR = H_{nr}; \qquad RH_IQ = H_{nr}, \tag{3.13c}$$

with (3.13a) governing the interactions between electron and radiation field, (3.13b) between electron and nucleus and (3.13c) between nucleus and radiation. According to [PÓ6], the electron-nucleus interaction Hamiltonian H_{en} is to first order of Coulomb type, the interaction thus being electric. Magnetic interaction contribute as well [PÓ6]. The respective Hamiltonians of both interaction types are:

$$H_{en} = \int \mathrm{d}^3 r_n \frac{\rho_n(\vec{r_n})}{|\vec{r_e} - \vec{r_n}|} \tag{3.14a}$$
$$H_{magn} = -\frac{1}{c}\vec{\alpha} \int \mathrm{d}^3 r_n \frac{\vec{j_n}(\vec{r_n})}{|\vec{r_e} - \vec{r_n}|}. \tag{3.14b}$$

In the latter formula we used the vector of Dirac matrices $\vec{\alpha} = (\alpha_x,\ \alpha_y,\ \alpha_z)$. Furthermore $\rho_n(\vec{r}_n)$ denotes the nuclear charge density, $\vec{j}_n(\vec{r}_n)$ the nuclear current, $\vec{r}_n$ the nuclear coordinate and $\vec{r}_e$ the electronic coordinate.

3.3 Expansion of the Transition Operator

The cross section for the process can be written as

$$\sigma_{i\to d\to f}(E) = \frac{2\pi}{F_i} \underbrace{\sum_{M_f m_d \varsigma} \int \mathrm{d}\Omega_{\vec{k}}}_{\text{sum over final states}} \underbrace{\frac{1}{2}\sum_{m_s} \frac{1}{2I_i+1} \sum_{M_i} \frac{1}{4\pi} \int \mathrm{d}\Omega_{\vec{p}}}_{\text{average over initial states}}$$
$$\times \lim_{\epsilon\to 0+} \left|\langle \Psi_f \left| T(E+i\epsilon) \right| \Psi_i \rangle\right|^2 \rho_f. \tag{3.15}$$

Herein the averaging over initial states refers to those states being not resolved in the experiment. F_i denotes the flux of incoming electrons, ρ_f the density of final photon states and $\Omega_{\vec{p}}$ and $\Omega_{\vec{k}}$ the direction of the incoming electron and outgoing photon in solid angle respectively.

In Equation (3.15) the reaction processes are described by the transition operator T. In this section we will focus on discussing the estimation of this quantity by Pálffy. T is derived in the framework of scattering theory, for which we refer to [Mer98], chapters 19 and 20, for a detailed description. There, the transition operator is given as

$$\langle f \left| T \right| i \rangle = \langle f \left| H_I \right| i \rangle + \sum_n \frac{\langle f \left| H_I \right| n \rangle \langle n \left| T \right| i \rangle}{E_i - E_n + i\epsilon}. \tag{3.16}$$

The states $|i\rangle$, $|f\rangle$ and $|n\rangle$ are eigenstates of the unperturbed Hamilton operator

$$H_0|n\rangle = E_n^0|n\rangle, \tag{3.17}$$

with $|i\rangle$ specifying an arbitrary initial state and $|f\rangle$ any possible final state for a choice of $|i\rangle$. This corresponds to the respective limits of a state long before and long after the scattering event. To formulate this limit in a sound fashion, the complex correction $i\epsilon$ of the energy in the

denominator of Eq. (3.16) had to be introduced. By the limit $\lim_{\epsilon\to 0+}$ introduced in the final cross section's equation (3.15) it will eventually vanish again.

The present form of the transition operator can be cast into a more usable form by introducing the Green's operators

$$G(z) = (z - H)^{-1} = \sum_n \frac{|n\rangle\langle n|}{z - E_n} = \sum_n \frac{|n\rangle\langle n|}{E - E_n + i\epsilon} \tag{3.18}$$

and

$$G_0(z) = (z - H_0)^{-1} = \sum_n \frac{|n\rangle\langle n|}{z - E_n^0} = \sum_n \frac{|n\rangle\langle n|}{E - E_n^0 + i\epsilon}, \tag{3.19}$$

where we introduced the complex energy variable $z = E + i\epsilon$ for brevity. Inserting this into the definition of the transition operator in Eq. (3.16) yields

$$\begin{aligned} T(z) &= H_I + H_I G_0(z) T(z) \\ &= H_I + H_I G_0 H_I + H_I G_0 H_I G_0 H_I + \ldots, \end{aligned} \tag{3.20}$$

omitting initial and final states in this step. This equation is one form of the *Lippmann-Schwinger equation*. Its recursiveness is the key property allowing the evaluation of the cross section to any order. As was already pointed out in section 3.1, NEEC is a resonant channel of photo recombination occurring only in association to a broad background of RR. This becomes also apparent in the evaluation of the various orders of the transition operator:

1st order:

$$\langle \Psi_f | RTP | \Psi_i \rangle = \langle \Psi_f | H_{er} | \Psi_i \rangle, \tag{3.21}$$

which represents radiative recombination.

2nd order:

$$\begin{aligned} \langle \Psi_f | RTP | \Psi_i \rangle &= \langle \Psi_f | H_I G_0 H_I | \Psi_i \rangle \\ &= \sum_q \frac{\langle \Psi_f | H_I | q \rangle \langle q | H_I | \Psi_i \rangle}{z - E_q} = \sum_q \frac{\langle \Psi_f | H_{nr} | q \rangle \langle q | H_{en} | \Psi_i \rangle}{z - E_q}, \end{aligned} \tag{3.22}$$

using the definition of G_0 and the multiindex q for the intermediate states which was first introduced in Eq. (3.7).

The further detailed expansion of the transition operator can be found in [PÓ6] in great detail and thus will not be redisplayed here.

3.4 Total Cross Section

The analysis of the expansion series of the transition operator inserted into the cross section's definition in Eq. (3.15) leads to the following expression for the cross section of NEEC followed by photon emission:

$$\begin{aligned} \sigma_{i\to d\to f} =& \frac{2\pi}{F_i} \int \mathrm{d}\Omega_{\vec{k}} \sum_{M_f m_{d\varsigma}} \frac{1}{2(2I_i + 1)} \sum_{m_s M_i} \frac{1}{4\pi} \int \mathrm{d}\Omega_{\vec{p}} \\ &\times \left| \sum_{M_d} \frac{\langle \Psi_f | H_{nr} | \Psi_d \rangle}{(E - E_d) + i\Gamma_d/2} \langle \Psi_d | H_{en} + H_{magn} | \Psi_i \rangle \right|^2 \rho_f. \end{aligned} \tag{3.23}$$

Γ_d is the width of the intermediate state (d), encompassing both internal conversion and photon emission as decay channels of the excited nucleus. Furthermore, E_d denotes the energy of the intermediate state. In the course of including the higher orders of the expansion of T, energy

corrections to this value due to polarization and self-energy of the nucleus as well as self-energy of the electron were included. The first order of the expansion of T, accounting for radiative recombination, has not been included here, as well as the interference term between NEEC and RR arising due to the squaring of the transition matrix element.

The form of Eq. (3.23) reveals that this formula can be separated into two rates connecting initial with intermediate and intermediate with final states of the system:

$$\begin{aligned}\sigma_{i\to d\to f}(E) =& \frac{2\pi}{F_i}\frac{1}{\Gamma_d}\underbrace{\frac{\Gamma_d}{(E-E_d)^2+{\Gamma_d}^2/4}}_{\propto \text{ Lorentzian profile}} \\ &\times \underbrace{\frac{1}{2(2I_i+1)}\sum_{M_i m_s}\sum_{M_d m_d}\frac{1}{4\pi}\int \mathrm{d}\Omega_{\vec{p}}\left|\langle\Psi_d|H_{en}+H_{magn}|\Psi_i\rangle\right|^2}_{\propto \text{ electron capture rate}} \\ &\times \underbrace{\frac{1}{2I_d+1}\sum_{M_f \varsigma}\sum_{M'_d}\int \mathrm{d}\Omega_{\vec{k}}\left|\langle\Psi_f|H_{nr}|\Psi_d\rangle\right|^2\rho_f}_{\propto \text{ radiative transition rate}}\,. \end{aligned} \tag{3.24}$$

More explicitly, we introduce the radiative transition rate as

$$A_r^{d\to f} = \frac{2\pi}{2I_d+1}\sum_{M_f \varsigma}\sum_{M'_d}\int \mathrm{d}\Omega_{\vec{k}}\left|\langle\Psi_f|H_{nr}|\Psi_d\rangle\right|^2\rho_f \tag{3.25}$$

and the electron capture rate as

$$Y_n^{i\to d} = \frac{2\pi}{2(2I_i+1)}\sum_{M_i m_s}\sum_{M_d m_d}\int \mathrm{d}\Omega_{\vec{p}}\left|\langle\Psi_d|H_{en}+H_{magn}|\Psi_i\rangle\right|^2\rho_i. \tag{3.26}$$

Herein we additionally introduced ρ_i as the density of initial continuum electronic states. The product of this quantity with the flux of impinging electrons of momentum p does not depend on the normalization of the continuum wave functions [Zim92],

$$F_i\rho_i = \frac{p^2}{(2\pi)^3}. \tag{3.27}$$

The Lorentzian profile normalized to unity is well known to be

$$L_d(E-E_d) = \frac{{\Gamma_d}/{2\pi}}{(E-E_d)^2+{\Gamma_d}^2/4}. \tag{3.28}$$

The occurrence of this line shape in the expression of the cross section in (3.24) highlights again the resonant nature of the process described here.

Together, equations (3.25) till (3.28) inserted into Eq. (3.24) give the following cross section formula:

$$\sigma_{i\to d\to f}(E) = \frac{2\pi^2}{p^2}\frac{Y_n^{i\to d}A_r^{d\to f}}{\Gamma_d}L_d(E-E_d). \tag{3.29}$$

The next section will be devoted to evaluating the afore defined transition rates $Y_n^{i\to d}$ and $A_r^{d\to f}$.

3.5 Evaluation of Transition Rates

3.5.1 Radiative Transition Rate

Formulas for radiative transitions in nuclei are already well known. Following [RS80] we use

$$A_r^{d\to f}(\lambda, L) = \frac{8\pi(L+1)}{L((2L+1)!!)^2}\left(\frac{E_n}{c}\right)^{2L+1} B(\lambda, L, I_d \to I_f). \tag{3.30}$$

Therein we denote the energy transferred to the nucleus as E_n, the multipolarity of the transition as L and its type as λ, which can be electric (E) or magnetic (M). Note that the double factorial occurring here does not denote factorial of factorial as one could think, but rather the factorial in the usual with only the odd or even numbers being included, depending on the argument being odd or even respectively. Furthermore, $B(\lambda, L, I_d \to I_f)$ is the *reduced transition probability* [RS80], which contains all information regarding the nuclear part of the transition. They are given in the form of reduced matrix elements:

$$B(E, L, I_d \to I_f) = \frac{1}{2I_i+1}\left|\langle N_f I_f||Q_L||N_d I_d\rangle\right|^2, \tag{3.31}$$

$$B(M, L, I_d \to I_f) = \frac{1}{2I_i+1}\left|\langle N_f I_f||M_L||N_d I_d\rangle\right|^2. \tag{3.32}$$

There the multipole operators for the electric (Q_L) and magnetic (M_L) transitions were introduced. Note that the dependency on magnetic quantum numbers does not occur any more in the expression (3.31) and (3.32) by virtue of the *Wigner-Eckart Theorem*, confer e.g. [GM96]. Reduced transition probabilities are furthermore compiled in *Weisskopf units* (WU) [RS80]. These comprise a numerical reference value depending on the type (E,L) or (M,L) of the transition and a dimension factor $e^2(fm)^{2L}$ for electric transitions and $\mu_N^2(fm)^{2L-2}$ for the magnetic ones. μ_N denotes therein the nuclear magneton $1/2mc$.

In principle the reduced transition probabilities can be calculated, relying thereby on theoretical models of the nucleus to circumvent the lack of detailed knowledge of nuclear wave functions. In order to avoid the approximative character of these models, one can rely instead on measured values where they exist. Experimental values for the reduced matrix elements are only available in the resolvable photon energy spectrum of the nucleus. Hence one has to rely again on an approximation in the domain of the continuum spectrum. This issue will be discussed in detail in chapter 4. Depending on the transition being either an excitation or a deexcitation, the correct direction of transition has to be chosen for the reduced transition probabilities as well. The modulus squared of the reduced matrix elements in Eq (3.31) and (3.32) does not depend on the direction of the transition in question. Therefore one can write

$$B\uparrow(\lambda L, I_d \to I_f) = \frac{2I_f+1}{2I_d+1} B\downarrow(\lambda L, I_f \to I_d). \tag{3.33}$$

3.5.2 Electron Capture Rate

After having discussed radiative transition rates we will now turn our attention towards the electron capture rate, which in section 3.4 was defined as

$$Y_n^{i\to d} = \frac{2\pi}{2(2I_i+1)} \sum_{M_i m_s} \sum_{M_d m_d} \int \mathrm{d}\Omega_{\vec{p}} \left|\langle \Psi_d | H_{en} + H_{magn} | \Psi_i\rangle\right|^2 \rho_i. \tag{3.34}$$

The definition of the electric as well as the magnetic interaction Hamiltonians were presented in Eq. (3.14). The evaluation of their matrix elements requires concepts of both atomic as well as nuclear physics.

The nuclear charge distribution $\rho_n(\vec{r_n})$ and the nuclear current $\vec{j_n}(\vec{r_n})$ are thus far unknown. To complete the theoretical treatment the *collective model* of the nucleus was introduced in [Pó6].

The collective model takes the phenomenological approach of approximating the nucleus as a charged liquid drop [RS80]. All the internal structure of the nucleus is not taken into account and instead a uniform density and composition of the nuclear matter is assumed. Only the shape and motion of the surface of the nucleus are treated. Starting from a stable configuration of the liquid drop as ground state of the nucleus, excited states are seen as rotations and vibrations

of the liquid drop. The simplest ground state configuration is given by the simple sphere, but deformed ground states are also possible.

This model allows one to connect the nuclear charge distribution $\rho_n(\vec{r_n})$ to the electric multipole moment Q_{lm} and the nuclear current $\vec{j_n}(\vec{r_n})$ to the magnetic multipole moment M_{lm}. The factors of $1/|\vec{r_e} - \vec{r_n}|$ under the integral of both transition Hamiltonians can be expressed by a multipole expansion. Together, this allows the separation of electronic and nuclear parts of the transition rates Y_n. Hence the nuclear matrix elements can again be expressed by the reduced nuclear transition probabilities (3.31) and (3.32).

The electron capture rate of electric type $Y_n^{E,L}$, which encompasses the H_{en} interaction, can be seen as the coupling between nuclear charge states and the charge of the continuum electron. Correspondingly, the electron capture rate of magnetic type $Y_n^{M,L}$ given by the H_{magn} interaction, are formulated as the interaction between the current formed by the continuum electron and its counterpart within the nucleus.

For the full scale derivation we again refer to the original work [PÓ6], from which we will only cite the final results for the electric and magnetic case respectively:

$$Y_n^{E,L} = \frac{4\pi^2\rho_i^2}{(2L+1)^2} B(E,L,I_i \to I_d)(2j_d+1) \sum_\kappa \left| R^{(E)}_{L,\kappa_d,\kappa} \right|^2 C(j_d L j;\ \frac{1}{2}0\frac{1}{2}), \tag{3.35}$$

$$Y_n^{M,L} = \frac{4\pi^2\rho_i}{L^2(2L+1)^2} B(M,L,I_i \to I_d)(2j_d+1) \sum_\kappa \left| R^{(M)}_{L,\kappa_d,\kappa} \right|^2 C(j_d j L;\ \frac{1}{2} - \frac{1}{2}0) \times \frac{(2j+1)}{2L+1}(\kappa_d + \kappa)^2, \tag{3.36}$$

with the electric and magnetic integrals

$$R^{(E)}_{L,\kappa_d,\kappa} = \int_0^\infty \mathrm{d}r_e\ r_e^{-L+1} \left[f_{n_d\kappa_d}(r_e) f_{\varepsilon\kappa}(r_e) + g_{n_d\kappa_d}(r_e) g_{\varepsilon\kappa}(r_e) \right], \tag{3.37}$$

$$R^{(M)}_{L,\kappa_d,\kappa} = \int_0^\infty \mathrm{d}r_e\ r_e^{-L+1} \left[g_{n_d\kappa_d}(r_e) f_{\varepsilon\kappa}(r_e) + g_{n_d\kappa_d}(r_e) f_{\varepsilon\kappa}(r_e) \right]. \tag{3.38}$$

Here $f_{\varepsilon\kappa}(r_e)$ and $g_{\varepsilon\kappa}(r_e)$ are components of the continuum electron wave function; ε is its energy measured from ionization threshold, defined by $\varepsilon = \sqrt{p^2c^2 + c^4} - c^2$. Furthermore, $f_{n_d\kappa_d}(r_e)$ and $g_{n_d\kappa_d}(r_e)$ are the respective components of the bound electron's wave function. The unindexed subscripts are used to denote states of the unbound electron. Wherever the index d appears we refer to a bound electron instead, as the electron in the intermediate step (d) got captured. For a detailed description of relativistic electron wave functions we refer the reader to [EM95]. Furthermore, we refer to the Clebsch-Gordan coefficients by $C(\cdot\,;\,\cdot)$.

Later we will draw again on Y_n. Then we will refer to it also by Γ_{NEEC}, the rate associated to excitation of the nucleus by NEEC.

4 Impact of NEEC on Stellar Nucleosynthesis

The formalism presented in chapter 3 can be used to derive the cross section of the two-step process of NEEC followed by photon emission. This cross section is proportional to the transition rate of NEEC.

To analyse the impact of NEEC on nucleosynthesis of heavy isotopes, we need to study a sequence of processes, which encompasses besides NEEC the initial neutron capture event, gamma-ray cascades and neutron re-emission. To this end we will investigate in section 4.3 the derivation of cross section expressions in a general, process-independent formalism, which will allow us to calculate all nucleosynthesis as well as NEEC reaction rates. Starting from these remarks we can incorporate in section 4.7 the NEEC rate into the frame of neutron capture nucleosynthesis introduced before in chapter 2.

4.1 NEEC in Nucleosynthesis Scenarios

In chapter 2, the nucleosyntheis of heavy isotopes was described by the ever-repeating sequence of the following steps:

1. Absorption of a free neutron by the nucleus resulting in an excited compound state. This is an excited state of a new isotope.

2. Deexcitation of the isotope in the compound state. Either the neutron is ejected again and the nucleus assumes its initial nucleon configuration again. Or the nucleus gamma-decays and thereby enters the ground state of the newly formed ground state.

3. If the nucleus in either case is unstable it may eventually decay to form a new isotope. Often this is beta-decay.

Hence NEEC can be incorporated into this framework in two basic scenarios, which are:

1. NEEC occurring before the initial capture of a neutron, so that the neutron is captured on an initially excited state and

2. NEEC built on the compound state of the nucleus formed by the initial neutron capture.

In the first case NEEC is leading to low excited states of the nucleus only. Yet these states are frequently populated by other mechanisms as well. The hot stellar plasma exhibits besides a great abundance of free electrons also an intense photon bath, which couples to the nucleus and causes population of low lying nuclear states as well. As the number of relevant nuclei in a star can be equally assumed to be large and to show a strong interaction with one another and the plasma, one can apply a statistical limit to these lower excited states and assume that they are in thermal equilibrium [BBK$^+$00]. In this manner, nucleosynthesis calculations incorporate the population of low-lying nuclear states already. Since thermal equilibration is therein assumed, the population densities of these states of low excitation energy are independent of the mode of transitions acting between them. Therefore we will not treat NEEC built on low-lying nuclear states. For simplicity we will also restrain ourself to the consideration of isotopes in their ground state and disregard isomeric states.

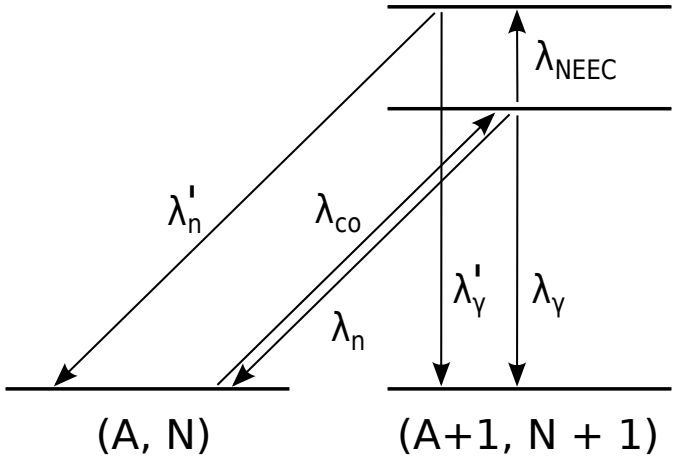

Figure 4.1: Considered transitions in the s-process nucleosynthesis of a new isotope including NEEC. The rates for formation of the compound state, neutron emission, gamma decay and NEEC are denoted by λ_{c0}, λ_n, λ_γ, λ_{NEEC}, respectively The primed rates denote the corresponding decay channels of the excited state reached via NEEC.

The alternative scenario is given by NEEC being built on the compound state of nucleus and captured neutron. The key point here is that the excited nuclear states occurring at initial neutron capture are of such high energy that they can not be assumed to be in thermal equilibrium. After neutron capture the nucleus has an energy of more than the separation energy of a neutron, which is of the order of several MeV. These states are very short lived, so that thermal equilibration can not occur. Hence, NEEC occurring between the initial capture of a continuum neutron and its decay might alter the effective cross sections associated to the different decay modes.

At excitation energies of several MeV as discussed in this scenario, the spectrum of the nucleus shows no resonance structure any more but rather enters a continuum regime. This continuum of excitations can be viewed as being caused by a quasi-continuous arrangement of nuclear levels. This is described by a level density approximation. An illustration of an exemplary level density approximation can be found in Fig. 4.3b; the details of the underlying model are outlined in the respective section. The density of states is much larger in the continuum spectrum compared to the resonance spectrum and is found to increase with increasing excitation energy. The probability of an excitation step built on the nuclear compound state is therefore larger compared to a deexcitation step. NEEC is one mechanism of such an additional excitation step together with photoabsorption, which has been investigated in this context by [BBB$^+$].

The full scenario we consider to quantify the impact of NEEC on nucleosynthesis has the following steps, which are depicted in Fig. 4.1:

- formation of the compound nucleus by neutron capture with rate λ_{co}
- the possible decay by neutron and photon emission of the compound nucleus with the associated rates λ_γ and λ_n
- alternatively the consecutive excitation of the compound nucleus by NEEC to a higher excited state with λ_{NEEC}
- the final decay of the second excited state via neutron emission or gamma decay (λ'_γ, λ'_n).

The experimental data of the steps induced by initial neutron capture are available in the form of cross section curves depending on the energy of the impinging neutrons. In the next two sections we will elaborate on measured neutron capture cross sections and give an overview over basic theoretical cross section expressions. This will also lead us to the setup of our calculations for the significance of NEEC for nucleosynthesis scenarios.

4.2 Cross Sections for Neutron Capture from Measurements

One difficulty faced upon calculating rates of neutron induced processes is that these rates are not directly measured in the usual neutron bombardment experiments. What one measures instead is the cross section of the net effects. These are the total cross section for formation of the compound nucleus, the (n, γ) cross section for the two-step process of initial neutron capture followed by gamma decay and (n, n') for neutron scattering. A subtlety involved in this is the nomenclature. Often the (n, γ) process is also referred to as neutron capture process, because the neutron is in this case permanently captured. Thereby the contrast to neutron scattering is emphasized, since in (n, n') the neutron does not stick inside the nucleus. To clearly separate (n, γ) neutron capture followed by gamma-decay from the one-step process of neutron capture simply leading to the excited compound state, the latter is always referred to as initial neutron capture within this work. Besides, the gamma decay does not necessarily bridge the whole energy gap down to the ground state by one single photon, but rather by two or more photons. Since levels in between can possibly serve as an intermediate state, a variety of γ *cascades* is possible.

A sample plot of these three cross sections as a function of the free neutron's energy is shown in Fig. 4.2. The data presented therein were taken from the [Lab11b] web interface, where measurements of the JENDL 4.0 data base [SIN$^+$11] were chosen. The discussion of the features of this cross section will be done for ^{187}Os, which we will also use as a sample isotope for our calculations. The respective plot of the cross sections of ^{187}Os is given to underline the variety of possible arrangements of the spectrum, although they bear the same fundamental features, and the need to adopt calculations to the isotope under consideration.

In the spectrum of ^{187}Os a clear resonance regime ranging to 1 keV in the continuum neutron's energy is visible, while the continuum spectrum above shows no such resonance feature. Additionally, the spectrum shows that up to approximately 10 keV the total cross section can be considered as being fully depleted by (n, γ) and elastic (n, n'). Thus, all other decay modes like fission and emission of protons, α-particles or inelastic scattered neutrons in various numbers, although in principle possible, can be safely neglected up to this energy. Other common nuclear decay mechanisms for low-lying nuclear levels such as IC are negligible at such high energies.

Above 10 keV, inelastic neutron scattering is an additional dominant decay mode competing with elastic neutron scattering and gamma decay. Both elastic neutron scattering and inelastic neutron scattering do not alter the composition of the nucleus, i.e. the decay of the compound nucleus leads in both cases back to the initial isotope. Hence inelastic scattering can be straightforwardly accounted for by adding its contribution to the elastic scattering one. By including inelastic neutron scattering all important contributing decay modes are accounted for up to energies of 100 keV. In the following we focus our attention on this energy window.

From the plotted cross sections in Fig. 4.2 it is also apparent that in the neighbourhood of the energetically lowest resonance peaks the (n, γ) cross section dominates the total cross section at large. For higher energies this situation is reversed completely and the (n, n') cross sections are significantly larger than the (n, γ) ones.

An excitation energy of the compound nucleus of more than ~ 10 keV via NEEC will exceed the neutron resonance spectrum and reach the continuum part. An optimal choice for the energy region to test the influence of NEEC on nucleosynthesis is therefore to built NEEC on one of the lower neutron resonances, so that the change in magnitude of the respective (n, n') and (n, γ) cross sections is very large.

To incorporate the NEEC rate into nucleosynthesis we need to formulate all reaction steps of nucleosynthesis as rates as well, i.e. the formation of the compound nucleus and gamma decay or neutron emission exiting the compound state. Yet some measured input is only available in the form of cross sections. We will present a review of general cross section considerations in the following to show how such cross sections can be appropriately translated into rates.

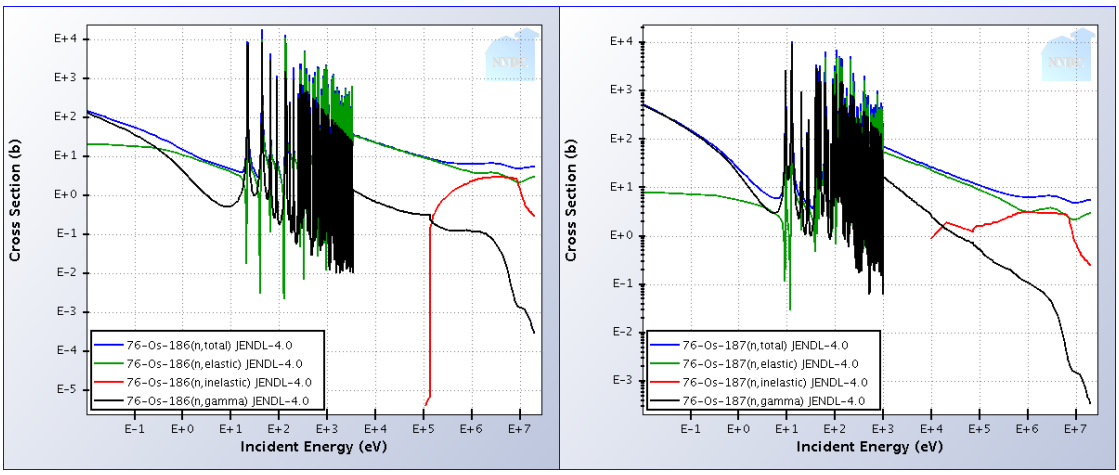

(a) ^{186}Os **(b)** ^{187}Os

Figure 4.2: Sample cross sections taken from [Lab11b]. See text for further explanation.

4.3 Theoretical Cross Section Expressions

The analysis presented here will mainly follow the discussion of Blatt and Weisskopf presented in [BW63]. The one-step cross section σ_{co} of the formation of an excited compound state by way of an excitation channel α of the nucleus can in general be given as

$$\sigma_{co}(\alpha) = \frac{\pi}{p^2} T(\alpha). \tag{4.1}$$

The prefactor of π/p^2, where p is the momentum of incoming particles, can be shown by simple geometric considerations to be the maximum possible cross section. The T is called *transmission coefficient* or *penetrability* of the channel α considered, depending on the transition being of decay or excitation type. It gives the probability of a particle to either escape the nucleus or enter it and form a compound state, respectively. The influence of angular momentum and spin will be neglected here. In the case of a resonance, this cross section expression is to be multiplied by a resonance envelope given by a Lorentzian profile $\mathcal{L}$

$$\mathcal{L}(E) = \frac{\Xi}{(E - E_{res})^2 + (\Gamma_{tot}/2)^2}, \tag{4.2}$$

with Ξ being the normalization constant, E_{res} defining the energy at resonance and Γ_{tot} the total width. The latter is given by the sum over all possible decay channels β:

$$\Gamma_{tot} = \sum_{\beta} \Gamma_{\beta}. \tag{4.3}$$

The average over several resonances has to be normalized to unity, which is well approximated by

$$D^{-1} \int_{-\infty}^{\infty} \mathcal{L}(E) \mathrm{d}E = 1. \tag{4.4}$$

D denotes the average level spacing here. This yields for the normalization constant Ξ the value $\Xi = D\Gamma_{tot}/2\pi$. The penetrability $T(\alpha)$ can be expressed by the corresponding width Γ_{α} via

$\Gamma_\alpha = T(\alpha)\frac{D}{2\pi}$ [BW63]. Together, this yields the desired cross section near resonance,

$$\begin{aligned}\sigma_{co}(\alpha) &= \frac{\pi}{p^2}T(\alpha)\mathcal{L} \\ &= \frac{\pi}{p^2}\frac{\Gamma_\alpha\Gamma_{tot}}{(E-E_{res})^2+(\Gamma_{tot}/2)^2}.\end{aligned} \tag{4.5}$$

This cross section for the capture process can be easily transformed into a cross section of a two-step process including also the decay via channel β by multiplying to it the branching ratio of the decay channel β under inspection,

$$\sigma(\alpha,\beta) = \sigma_{co}(\alpha)\frac{\Gamma_\beta}{\Gamma_{tot}} = \frac{2\pi^2}{p^2}\frac{\Gamma_\alpha\Gamma_\beta}{\Gamma_{tot}}\frac{\Gamma_{tot}/2\pi}{(E-E_{res})^2+(\Gamma_{tot}/2)^2}. \tag{4.6}$$

In this way excitation and decay are incorporated into the cross section.

The concept introduced in Equations (4.1) and (4.6) form the basis of many stellar reaction model calculations. For example, such considerations are required for the calculation of the Maxwellian-averaged cross sections mentioned in section 2.4 (confer Ref. [FMM$^+$10, RT00]).

Using Equation (4.6) the branching ratio introduced therein can then of course also be calculated via

$$\frac{\Gamma_\beta}{\Gamma_{tot}} = \frac{\sigma(\alpha,\beta)}{\sigma_{tot}}, \tag{4.7}$$

whereby $\sigma_{tot} = \sigma_{co}(\alpha) = \sum_\beta \sigma(\alpha,\beta)$ [BW63].

Starting from an expression for the cross section one can obtain the rate by which the process occurs via

$$\lambda = \int \sigma(E)\phi(E)\mathrm{d}E. \tag{4.8}$$

Therein the flux ϕ of incoming particles was incorporated. Note that these reaction rates λ are not equivalent to the rates denoted as Γ in Eq. (4.6).

Utilizing the concepts presented in the last two sections, we proceed to calculate the rates associated to all steps of nucleosynthesis combined with NEEC in the next two sections.

4.4 Formation and Decay of the Compound State

In this section we want to summarize the expressions used to calculate the rates of the formation of the compound state and gamma decay of the compound state as well as neutron emission.

In section 4.3, Γ_β was introduced as the width associated to the respective spontaneous de-excitation process; in the atomic units this is equivalent to the rate of decay. While Γ_β can be used in the rate equations, the rate of initial excitation Γ_α depends on the flux of neutrons present in the environment of the considered process. The rate of compound nucleus formation λ_{co} is in this case obtained via Eq. (4.8). For the neutron flux we adopted the parametrization of [BBK$^+$00], where compound nucleus formation is treated for the calculation of the afore mentioned Maxwellian-averaged stellar cross sections. The neutrons are treated as classical, non-relativistic particles in thermal equilibrium so that they obey a Maxwell-Boltzmann distribution Φ_{MB}

$$\Phi_{MB}(v)\mathrm{d}v = \frac{4}{\sqrt{\pi}}\left(\frac{v}{v_T}\right)^2\exp\left(-\frac{v}{v_T}\right)^2\mathrm{d}\left(\frac{v}{v_T}\right) \tag{4.9}$$

with $v_T = \sqrt{2kT/m}$ being the mean thermal velocity and m the reduced mass of the combined neutron-target system.

In this context a slight variation of (4.8) is used,

$$\lambda_{co} = \int \sigma(v)\phi_n(v)\mathrm{d}v, \tag{4.10}$$

with the flux of impinging neutrons being defined as

$$\phi_n(v) = n_n v \Phi_{MB}(v). \tag{4.11}$$

We denote the stellar neutron particle density by n_n, whose value can be taken from theoretical stellar models or approximations derived from astronomical observation. The nucleosynthesis process incorporating ^{187}Os, which we will adopt as our model isotope, is the s-process. The site of the s-process is the stellar interior with a relatively low neutron flux. Käppeler et al. [KBW89] estimated the neutron density n_n from astronomical observation data to be around $2 \cdot 10^8$ 1/cm^{-3}. This value will be adopted in our calculations.

The cross section required in the calculation of λ_{co} is the cross section of the formation of the compound state σ_{co}. In section 4.3 this was shown to be equivalent to the total cross section σ_{tot} at the respective energy.

The rates λ_β of decay of the compound state into channel β was shown to be given by the width Γ_β of the respective channel. These rates are not obtainable by the manipulation of the respective measured cross sections, because these cross sections always comprise the two-step process of absorption and decay. Yet Eq. (4.6) reveals that the widths Γ_β are nonetheless captured within the cross section, as long as a resonance peak is treated. As becomes apparent from (4.6) the width of a resonance peak is given by the total width Γ_{tot} for any kind of decay channel. Yet the width Γ_β of the channel of decay β is captured in the height of the resonance peak and is thus also obtainable. All these resonance parameters are tabulated; we used the compendium [MDH81].

Though the width of the neutron ejection decay is tabulated for all the resonances of interest, the gamma decay width often is not. In such cases we apply a general consideration of Blatt and Weisskopf [BW63] to the gamma-decay rate. They observe that for energies of nuclear excitation through initial neutron capture up to 0.5 MeV above neutron separation energy and heavy nuclei, the gamma-decay width stays remarkably constant. They assign to Γ_γ a value of 0.1 eV.

By virtue of the discussion above the rates of neutron absorption, gamma decay from the compound state and neutron emission from the compound nucleus are obtainable. In the next section we will turn towards the calculation of the NEEC rate and the decays of the nuclear state thus reached.

4.5 NEEC following Neutron Capture

In chapter 3, an expression for the cross section of NEEC followed by photon emission built on the nucleus's ground state was derived, see Eq. (3.29). From the discussion presented in section 4.3 it now becomes clear that this cross section obeys exactly the general expression presented in Eq. (4.6). Hence the transition rates appearing in (3.29) remain valid independently of the setting to which they were prescribed in section 3 and can be reutilized in any new cross section of the form of (4.6).

With the help of the latter equation we will formulate a rate for the combined processes of NEEC followed by decay into any considered channel. This treatment is necessary because one can not easily derive the decay rates from the nuclear state after NEEC occurred. This impasse is avoided by combining the step of excitation through NEEC with the consecutive deexcitation into a new cross section according to (4.6). The two-step cross section is given by

$$\begin{aligned}\sigma_{\mathrm{NEEC}+\beta}(E) &= \frac{2\pi^2}{p^2}\Gamma_{\mathrm{NEEC}}\frac{\Gamma_\beta}{\Gamma_{tot}}\frac{\Gamma_{tot}/2\pi}{(E-E_{res})^2+(\Gamma_{tot}/2)^2} \\ &= \frac{2\pi^2}{p^2}\Gamma_{\mathrm{NEEC}}\frac{\sigma_\beta}{\sigma_{tot}}\frac{\Gamma_{tot}/2\pi}{(E-E_{res})^2+(\Gamma_{tot}/2)^2},\end{aligned} \tag{4.12}$$

for the decay mode β being either gamma or neutron emission. The values for σ_β and σ_{tot} can be taken from experimental data as discussed above. Using the flux of free electrons and the

cross section $\sigma_{\mathrm{NEEC}+\beta}$ above one can obtain the rate of the considered unified two-step process by utilizing Eq. (4.8).

The expression for the electron flux can be inferred by assuming that the electrons are in thermal equilibrium like the neutrons and follow a Fermi-Dirac distribution. The same assumption was taken by Gosselin et al. [GM04] in their treatment of NEEC in astrophysical environments. Considering the electrons to be relativistic, the influx of electrons ϕ_e is given by

$$\phi_e(E_{\mathrm{cont}}) = \underbrace{\frac{c}{2\pi^2}\frac{{E_{\mathrm{cont}}}^2}{(c\hbar)^3}}_{\text{Density of states}} \times \underbrace{\frac{1}{1+\exp\left(E_{\mathrm{cont}}/k_B T\right)}}_{\text{Fermi-Dirac distribution}} . \tag{4.13}$$

Here E_{cont} is the energy of the continuum electrons captured by the atom, k_B the Boltzmann constant and T the temperature of the stellar plasma. The form of ϕ_e is again adopted from [GM04]; the density of states has this form for relativistic particles [PB11].

For the calculation of the combined rate of NEEC followed by decay, the reduced transition probabilities B are needed. As argued in section 3.5.2 for low-energy transitions, the adoption of a measured value would be the best choice, because theoretical parametrizations of the nucleus always rely on rather rough approximations. Unfortunately, such measured values are not available for high nuclear excitations as discussed here, where the nuclear spectrum shows a continuum character. Therefore we have to introduce an approximative model for the nuclear transition. This will be discussed in the next section.

4.6 Reduced Transition Probabilities for Highly Excited Nuclear States

The estimation of the reduced transition probability B for transitions of low energy in the unresolved nuclear energy spectrum presents a great uncertainty, because no model has been developed to treat them specifically. In the following we introduce two different approximate approaches and will compare the numerical results obtained by both estimates.

4.6.1 Estimate from Photon Strength Function

Nuclei exhibit in the continuum regime of the photon spectrum a *giant resonance* [GM96]. In its dominant and simplest form it is of an electric dipole type and can be described as a collective motion of neutrons versus protons. This nuclear mode, called giant dipole resonance (GDR), can be induced by excitation energies between 10 and 20 MeV and envelopes an energy range of several MeV. In the photon spectrum of the nucleus this is the dominant excitation feature and hence attracted a lot of interest [Bec09, BCCK92]. In the simple picture of a collective motion of neutrons versus protons, the nuclear matter in fact acts like a dipole resonator. Therefore it is not surprising that this spectrum can be well approximated by a Lorentzian shape [Jac62]. In the case of an axially symmetric, deformed nucleus one can often distinguish between two different directions of the collective motion, giving rise to the double-Lorentzian shape depicted in Fig. 4.3a, where the photon strength function for ^{187}Os is depicted. In this case the two peaks turn out to be very narrow. The expression for the photon strength function as discussed above is

$$S_{E1}(E_\gamma) = \frac{1}{3\pi^2(\hbar c)^2}\sum_{i=1}^{2}\frac{\sigma_i {E_\gamma}{\Gamma_{Gi}}^2}{\left({E_\gamma}^2 - {E_{Gi}}^2\right)^2 + {E_\gamma}^2{E_{Gi}}^2}, \tag{4.14}$$

where E_{Gi} is the central energy of the axial branch i of the GDR and Γ_{Gi} its damping width [Bec09, SS67]. Furthermore the transition energy was therein denoted by E_γ.

In 1955 Brink proposed that such a giant dipole resonance can in fact be built on every excited nuclear state, not just the ground state, retaining its exact shape as is found for the ground state-GDR [Bri55].

The interaction of a photon with a nucleus in the continuum spectrum of the nucleus is parametrized by photon strength functions, which describe the shape of the spectrum. The hypothesis of Brinkman is usually taken to hold [Bec09], so that the photon strength function S of the electric giant dipole resonance relates to the expectation value of the transition of gamma-decay as

$$\overline{\Gamma}(E_x + E_\gamma \to E_x) = \frac{{E_\gamma}^3 S(E_\gamma)}{\rho(E_x + E_\gamma)}. \tag{4.15}$$

Here $\rho(E_x + E_\gamma)$ is the level density of the upper level. The strength function is independent of the levels between which the transition occurs as a consequence of the Brink hypothesis. Applying the principle of detailed balance one can easily derive the appropriate relationship for the inverse, upwards transition

$$\overline{\Gamma}(E_x \to E_x + E_\gamma) = \frac{{E_\gamma}^3 S(E_\gamma)}{\rho(E_x)}. \tag{4.16}$$

The energy of the lower involved level is represented by E_x.

Of the variety of models and their parametrizations describing the density of states we employed the *Back-shifted Fermi gas model* in the spin-independent form taken from [EB05]

$$\rho(E) = \frac{\exp 2\sqrt{a(E-\Delta)}}{12\sqrt{2}\chi a^{1/4}(E-\Delta)^{5/4}}, \tag{4.17}$$

with a being the single-particle density parameter, Δ the backshift and χ the spin cutoff parameter, given by

$$\chi^2 = 0.0146A^{5/3}\frac{1+\sqrt{1+ta(E-\Delta)}}{2a}. \tag{4.18}$$

In Ref. [EB05] also the associated fitted parameters for a great number of isotopes is given. For ^{187}Os the curve of $\rho(E)$ is depicted in Fig. 4.3b.

The rate defined by Eq. (4.16) is the average photon deexcitation rate in the considered energy regime. This can be set equal to the known gamma rate for nuclear transition as it was introduced in Eq. (3.30), which yields the required value of the reduced transition probability as

$$B(E_x, E_\gamma) = \frac{(3!!)^2 c^3}{4}\frac{S(E_\gamma)}{\rho(E_x)} \qquad \text{for } L = 1. \tag{4.19}$$

There the multipolarity of the transition was already set to unity for the GDR. In the actual calculation it has to be remembered that the B-value has to be given in the correct Weisskopf units as introduced in section 3.5.1.

In our considerations the NEEC transition energy is less than $E_\gamma = 100$ keV, while the photon strength function $S(E_\gamma)$ used in the presented estimate of B is only experimentally established for transition energies on the MeV scale. To extract the photon strength function to such low transition energies is therefore a very uncertain and rough estimate.

4.6.2 Estimate from Sum Rule

An alternative approximation for the reduced transition probability was derived by [BW63]. In its dipole form this expression assumes the form

$$B(E_x, E_\gamma) = \left(\frac{3}{4}\right)^2 \frac{e^2R^2}{4\pi}\rho_0\ \rho(E_x + E_\gamma). \tag{4.20}$$

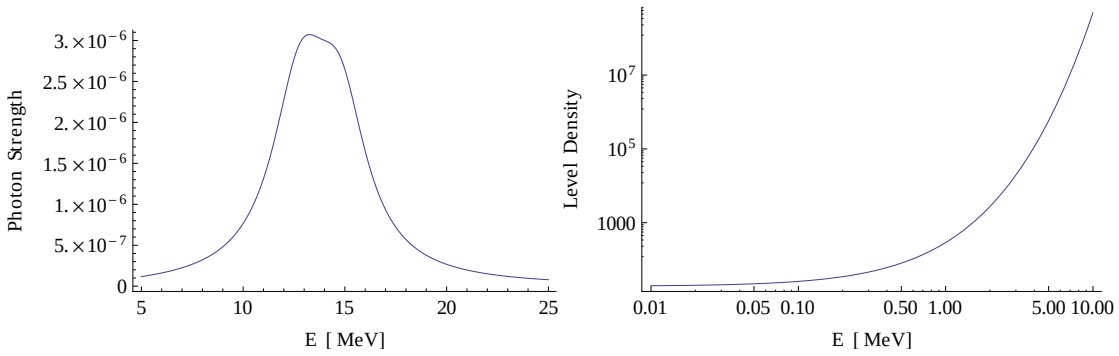

(a) Photon Strength Function **(b)** Level Density

Figure 4.3: Visualization of the parameterizations of the the photon strength function (a) and the back-shifted Fermi gas approximation of the level density (b) for ^{187}Os.

Herein R denotes the nuclear radius, ρ the density of states as introduced in the discussion of the alternative estimate and ρ_0 the level density of low-lying nuclear levels. For heavy nuclei this can taken to be ~ 0.1 MeV.

The nuclear radius can be calculated with te help of the expression [JS85]

$$R = (1.0793A^{1/3} + 0.73587)\ \text{fm}, \tag{4.21}$$

with A being the atomic mass number.

Blatt and Weisskopf themselves note on the validity of their estimate of the reduced transition probability, though, that it is possibly only very vague.

4.7 Rate Equation Network Calculation

As mentioned in the previous section, the NEEC transition of the compound state nucleus prior to decay to the ground state is incorporated into a joint reaction rate together with the decay of the compound nucleus excited by NEEC. Thereby only three stages remain in the production of a new isotope starting from its predecessor in ground state. These are identical for both scenarios with and without NEEC and are:

- the initial isotope (A, N) in its ground state, in the following labelled N_1,
- the isotope after initial neutron capture in the compound state $(A+1, N+1)^*$, in the following labelled N_2,
- the isotope $(A+1, N+1)$ in its ground state, in the following labelled N_3.

The time evolution of a system as presented above can be studied with the network of rate equations describing the occupation of every state. A rate equation is a first order linear differential equations, taking into account all rates populating and depleting a state. This gives the following set of rate equations for our system of stages of nucleosynthesis:

$$\frac{\mathrm{d}N_1(t)}{\mathrm{d}t} = -\lambda_{co}N_1(t) + (\lambda_n + \lambda_{\text{NEEC}+n})N_2(t), \tag{4.22a}$$

$$\frac{\mathrm{d}N_2(t)}{\mathrm{d}t} = \lambda_{co}N_1(t) - (\lambda_n + \lambda_{\text{NEEC}+n} + \lambda_\gamma + \lambda_{\text{NEEC}+\gamma})N_2(t), \tag{4.22b}$$

$$\frac{\mathrm{d}N_3(t)}{\mathrm{d}t} = (\lambda_\gamma + \lambda_{\text{NEEC}+\gamma})N_2(t), \tag{4.22c}$$

with the initial conditions set to be

$$N_1(0) = N_1^{\text{initial}}; \qquad N_2(0) = 0; \qquad N_3(0) = 0. \tag{4.22d}$$

Here we denoted the rates of NEEC followed by decay as $\lambda_{\text{NEEC}+\gamma}$ and $\lambda_{\text{NEEC}+n}$, respectively.

It is not considered here that the initial isotope N_1 has in reality an input rate and N_3 an exit rate as well, because both are part of an overall nucleosynthesis path. Instead, we assume for our calculations an arbitrary initial occupation of N_1, called N_1^{initial}, and investigate the change in the level occupations as a function of time. Furthermore, we assumed in Eq. (4.22d) that both other levels are unoccupied at initial time $t = 0$. While this is realistic for N_2, which is only a transitional state, this can be only seen as a first approximation for stars of younger generation where the matter contains metal impurities synthesized by earlier generations. The form of Equation (4.22c) reveals already that a built-up of the N_3 occupation will happen and the level N_1 will be depleted with evolving time. Our measure for the impact of NEEC on the s-preocess nucleosynthesis of the isotope under consideration will therefore be the timescale by which the occupation of the newly formed isotope N_3 builds up. In this simple scenario the initial occupation of N_3 is completely irrelevant and can be safely set to zero.

The impact of NEEC on nucleosynthesis scenarios is most significant it the rates of NEEC followed by deexcitation are able to shift the number of nuclei decaying by gamma emission compared to those decaying by neutron emission decisively, in other words if the net branching ratios are notably changed. Another aspect is the change in net rate of decay modes leading either to gamma emission or to neutron emission. A notable change of these would modify the nucleosynthesis yield as well, as the effective lifetime of the remaining intermediate excited state would be quenched, even if the afore mentioned branching ratios remain roughly the same.

The transition energy E_γ and the lower state energy E_x of the nucleus will be chosen such as to ensure a maximum possible influence of NEEC as discussed above. Thereby E_x is determined by the kinetic energy of the continuum neutron at resonance. In total the neutron transfers its kinetic energy and the neutron separation energy to the nucleus, thus yielding E_x. The neutron separation energy is defined as the energy a neutron has at least to gain in order to be able to exit the nucleus. In the case of ^{187}Os this is 6.29 MeV.

5 Numerical Results

Here we present our numerical results for a first estimate of the impact of nuclear excitation by electron capture on neutron capture nucleosynthesis. While this excitation mechanism is already implicitly accounted for for low-lying excited states, NEEC built on the nuclear compound state presents a novelty in nucleosynthesis considerations. As a test case we have chosen ^{187}Os, an isotope of special importance. The nuclear properties of the isotopes in the Re/Os region allow the determination of the age of the universe, for which the precise as possible knowledge of the neutron capture and neutron emission behaviour in stellar environments is necessary. ^{187}Os is a stable isotope included in the s-process.

Our results encompass a first study of the coupling of the nucleus to the atomic shell in stellar plasmas involving highly excited nuclear states. It serves to illustrate the possible impact and give possible directions of further investigations.

5.1 Calculation of NEEC Transition Rates

We consider the electron capture to occur into the lowest unoccupied level for different degrees of ionization, corresponding to bare, Li-like, B-like and N-like ionic configurations. The respective shells into which capture occurs are $1s_{1/2}$, $2s_{1/2}$, $2p_{1/2}$ and $2p_{3/2}$ belonging to the K and L-shells are treated. The respective bound electron energies are presented in Tab. 5.1 Whether the temperature of the stellar interior suffices to yield the respective degree of ionization is for now not investigated.

Ionization Degree	nl_j	E_{bound} [keV]	E_γ [keV]
Bare	$1s_{1/2}$	-85.6	90
Li-like	$2s_{1/2}$	-20.9	90; 30
B-like	$2p_{1/2}$	-20.1	90; 30
N-like	$2p_{3/2}$	-17.4	90; 30

Table 5.1: Considered configurations of electron capture. The notation nl_j is used to symbolize the atomic orbital into which electron capture occurs. The energy of the state is given by E_{bound}, while E_γ is the chosen nuclear transition energy for NEEC.

In order to calculate the NEEC transition rates, the bound and continuum radial wave functions of the electron need to be known and numerically integrated to yield the electric and magnetic radial integrals $R^E_{L,\kappa_d,\kappa}$ and $R^M_{L,\kappa_d,\kappa}$ given by Eq. (3.37).

The continuum electron is assumed to be insensitive to the internal structure of the nucleus; relativistic Coulomb-Dirac wave functions are used [EM95], taking the further approximation of a point-like nucleus. This concerns the initial electron wave function, while the final, captured electron's wave function are specifically calculated for every case using the GRASP92 package [PFG96]. This code allows the calculation of relativistic bound state wave function with a multiconfigurational Dirac-Fock approximation and includes the treatment of the nucleus as an extended, spherically symmetric source as well as QED corrections to the energy levels.

The thus obtained bound electron wave functions are assumed to be valid also in a plasma environment. This is only approximative as the plasma couples to the atomic orbitals and induces shifts to the solution for an independent ion.

Besides the radial wave functions of continuum and bound electron states, the calculation of the NEEC transition rate additionally requires the determination of the reduced transition probability B. As already discussed in chapter 4, two theoretical, approximative approaches are taken into consideration. These are the estimate derived from the photon strength function of the giant dipole resonance on one hand and the alternative estimate from sum rules.

Both approximations of B require an estimate for the level density in the regime of high excitation energies. This was in section 4.6.1 taken to be given by the back-shifted Fermi gas model. The required input parameters for the density of states in Eq. (4.17) are taken from the same source as the expression itself [EB05] and are

$$\Delta = -0.78 \text{ MeV}; \qquad a = 19.07 \text{ MeV}^{-1} \tag{5.1}$$

for ^{187}Os.

The approximation of B using the photon strength function additionally needs parameters for the double-Lorentzian approximation of the GDR. These can be taken from [SS67]. Unfortunately there is currently no GDR parametrization available for ^{187}Os. We will follow the proposal of [FMM$^+$10], where the role of ^{187}Os and others within the Re/Os clock was extensively studied, and use the photon strength function of ^{189}Os instead. This is the nearest stable isotope of osmium to ^{187}Os and is also an odd-A isotope. Because the nuclear properties of odd-A and respectively even-A nuclei are often closer to allied nuclei belonging to the same type than to nuclei of the other type, this choice appears as the most reasonable one. The chosen values are presented in Tab. 5.2.

Γ_{G1} [MeV]	E_{G1} [MeV]	σ_1 [b]	Γ_{G2} [MeV]	E_{G2} [MeV]	σ_2 [b]
3.39	12.93	0.334	3.19	14.86	0.314

Table 5.2: Photon strength function parameters of ^{189}Os, adopted for ^{187}Os. These values are used in expressions (4.14).

Taking these models together we have all required information at hand to calculate the transition rate Γ_{NEEC} of NEEC. Together with the obtained values for B its numerical values are tabulated in 5.5 and 5.6.

5.2 Reaction Rates

As is shown in Tab. 5.1, all bound electron energies are of the order of keV. The bound electron's energy is also the minimum energy transferred to the nucleus, such that the nuclear transition induced by NEEC on the compound nucleus necessarily shifts the nuclear energy into the neutron continuum spectrum of the nucleus. Sample neutron cross section spectra are displayed in Fig. 4.2. These spectra reveal that in the continuum region the elastic and inelastic neutron scattering channels contribute most to the total cross section, while the neutron capture mode gives only a minor contribution. The inverse situation can be found for the first resonances at very low neutron energy. Therefore we expect NEEC to have the most significant effect in the considered scenario if the free neutron captured by the nucleus has only very low energy, so that one of the first resonances is excited. We chose the first resonance of ^{187}Os at 9.47 eV.

Upon initial neutron capture, neutron and nucleus form a compound state, on which NEEC can occur. Since the binding energies of the electrons differ a lot between capture into K-shell and capture into L-shell, two different NEEC transition energies were investigated, namely 30 and 90 keV, as is shown in Tab. 5.1. The transition energies were chosen such that the continuum electron's energy is low for every considered capturing shell. To allow a better comparison, both continuum electron energies were investigated where possible.

Additionally we assumed in our estimates no energy spread for both free neutrons and electrons, which is a rough approximation given the plasma environment. This corresponds to an

infinitesimal thin resonance peak, which is given by a delta distribution. Incorporating this simplification into the general formulae for two-step cross sections (4.6) and associated reaction rates (4.8) yields the expressions:

$$\begin{aligned}\sigma_{\alpha,\beta}(E) &= \frac{2\pi^2}{p^2}\frac{\Gamma_\alpha\Gamma_\beta}{\Gamma_{tot}}\frac{\Gamma_{tot}/2\pi}{(E-E_{res})^2+(\Gamma_{tot}/2)^2} \\ &\xrightarrow{\Gamma_{tot}\to 0} \frac{2\pi^2}{p^2}\frac{\Gamma_\alpha\Gamma_\beta}{\Gamma_{tot}}\delta(E-E_{res}) \end{aligned} \tag{5.2}$$

and

$$\begin{aligned}\lambda &= \int \sigma_{\alpha,\beta}(E)\phi(E)\mathrm{d}E \\ &\to \int \frac{2\pi^2}{p^2}\frac{\Gamma_\alpha\Gamma_\beta}{\Gamma_{tot}}\delta(E-E_{res})\phi(E)\mathrm{d}E \\ &= \frac{2\pi^2}{p^2}\frac{\Gamma_\alpha\Gamma_\beta}{\Gamma_{tot}}\bigg|_{\text{at resonance}} \times \phi(E_{res}). \end{aligned} \tag{5.3}$$

For the formation of the compound state in accordance with Eq. (4.10) and the associated discussion, the latter equation takes the form

$$\lambda_{co} = \sigma_{tot}(v)\phi_n(v)n_n v\Phi_{MB}(v)|_{\text{at resonance}}\,. \tag{5.4}$$

The values for the neutron cross sections are taken from the JENDL 4.0 data base [SIN+11] via the [Lab11b] web interface. The appropriate cross section value for λ_{co} can be found in Tab. 5.4. The neutron flux n_n of s-process stellar environments is taken from [KBW89] as approximately $2 \cdot 10^8$ 1/cm^{-3}. Together, this yields for the reaction rate of compound nucleus formation the value

$$\lambda_{co} = 9.97\ 10^{-12} s^{-1}. \tag{5.5}$$

The rates of direct decay from the compound state are regarded as independent of any external particle flux. Hence these rates are given by the widths Γ_β of the respective decay mode β. These neutron resonance parameters were taken from [MDH81]. They are:

Γ_γ [meV]	λ_γ [s^{-1}]	$2g\Gamma_n$ [meV]	λ_n [s^{-1}]
81	1.23 10^{14}	2.61	3.97 10^{12}

Table 5.3: Resonance parameters of the ^{187}Os resonance at $E_{res} = 9.47$ eV and thereof caculated rates. [MDH81]

The statistical weight factor g appearing in the third column of Tab. 5.3 depends on the nuclear spin state, which we do not include into our considerations and is therefore set to $2g = 1$.

The last reaction rates we need to consider are the rates of combined NEEC and decay of the newly reached nuclear state. Again, only gamma-decay and neutron emission are considered as possible decay channels after NEEC. As was discussed in section 4.2, these are the main contributions to the total cross section in the considered energy range of nuclear excitation. In Tab. 5.4 the required cross section values at the energies investigated are listed.

The rates of NEEC followed by decay into channel β are calculated via

$$\lambda_{\text{NEEC}+\beta} = \frac{2\pi^2}{p^2}\Gamma_{\text{NEEC}}\frac{\sigma_\beta}{\sigma_{tot}}\phi(E_{cont}), \tag{5.6}$$

with the flux of free electrons given as in Eq. (4.13). The numerical values for the respective cross sections are taken from Tab. 5.4. Note that for all energy values included in our discussions

E	$E_n = 9.47$ eV	$E_n + 30$ keV	$E_n + 90$ keV
σ_{tot} [b]	$2.54\ 10^3$	17.2	11.6
σ_n [b]	-	16.2	10.9
σ_γ [b]	-	1.8	$5.7\ 10^{-1}$

Table 5.4: Cross section values for the considered energy values. The energy E is the one of the continuum neutron. The values were obtained from [SIN+11].

the cross sections of the particular decay modes almost add up to the total cross section. The remaining fractions contribute to a variety of other decay modes which are taken to be negligible here.

The numerical values for all reaction rates and both approximations of the reduced transition probability are given in Tab. 5.6 and 5.5 for a stellar temperature of $k_BT = 30$ keV.

	$E_\gamma = 30$ keV				$E_\gamma = 90$ keV			
	B [WU]	Γ_{NEEC}	$\lambda_{\mathrm{NEEC}+\gamma}$	$\lambda_{\mathrm{NEEC}+n}$	B [WU]	Γ_{NEEC}	$\lambda_{\mathrm{NEEC}+\gamma}$	$\lambda_{\mathrm{NEEC}+n}$
$1s_{1/2}$	-	-	-	-	$3.15\ 10^{-6}$	$1.27\ 10^4$	$3.75\ 10^{15}$	$7.18\ 10^{16}$
$2s_{1/2}$	$3.43\ 10^{-6}$	$3.94\ 10^4$	$4.70\ 10^{16}$	$4.23\ 10^{17}$	$3.15\ 10^{-6}$	$4.75\ 10^5$	$4.08\ 10^{17}$	$7.80\ 10^{18}$
$2p_{1/2}$	$3.43\ 10^{-6}$	$1.90\ 10^6$	$2.43\ 10^{18}$	$2.18\ 10^{19}$	$3.15\ 10^{-6}$	$3.87\ 10^6$	$3.28\ 10^{18}$	$6.27\ 10^{19}$
$2p_{3/2}$	$3.43\ 10^{-6}$	$4.24\ 10^6$	$6.52\ 10^{18}$	$5.86\ 10^{19}$	$3.15\ 10^{-6}$	$7.86\ 10^6$	$6.36\ 10^{18}$	$1.22\ 10^{20}$

Table 5.5: Obtained values for the sum rule model and a stellar temperature of $k_BT = 30$ keV. All rates are given in dimensions of [1/s]. The ionization degrees were chosen as indicated in Tab. 5.1.

	$E_\gamma = 30$ keV				$E_\gamma = 90$ keV			
	B [WU]	Γ_{NEEC}	$\lambda_{\mathrm{NEEC}+\gamma}$	$\lambda_{\mathrm{NEEC}+n}$	B [WU]	Γ_{NEEC}	$\lambda_{\mathrm{NEEC}+\gamma}$	$\lambda_{\mathrm{NEEC}+n}$
$1s_{1/2}$	-	-	-	-	$1.20\ 10^{-10}$	0.48	$1.43\ 10^{11}$	$2.74\ 10^{12}$
$2s_{1/2}$	$3.97\ 10^{-11}$	0.46	$0.54\ 10^{12}$	$4.90\ 10^{12}$	$1.19\ 10^{-10}$	$1.79\ 10^1$	$1.54\ 10^{13}$	$2.95\ 10^{14}$
$2p_{1/2}$	$3.93\ 10^{-11}$	$2.19\ 10^1$	$2.78\ 10^{13}$	$2.50\ 10^{14}$	$1.18\ 10^{-10}$	$1.45\ 10^2$	$1.23\ 10^{14}$	$2.35\ 10^{15}$
$2p_{3/2}$	$3.89\ 10^{-11}$	$4.81\ 10^1$	$7.40\ 10^{13}$	$6.65\ 10^{14}$	$1.17\ 10^{-10}$	$2.91\ 10^2$	$2.36\ 10^{14}$	$4.50\ 10^{15}$

Table 5.6: Obtained values for the photon strength model and a stellar temperature of $k_BT = 30$ keV. All rates are given in dimensions of [1/s]. The ionization degrees were chosen as indicated in Tab. 5.1.

The estimate for the reduced transition probability B from sum rules turns out to be around 4 orders of magnitude larger than the estimate based on the photon strength function. None of these estimates can be preferred from our discussions, so that this difference has to be taken as a benchmark of the uncertainty involved in our calculations. It furthermore underlines the qualitative nature of our discussion. In the following we will us the B estimate derived from the photon strength function. This approach gives the lower numerical results and thus appears as the more timid choice.

Even for this choice NEEC shows a notable impact. For capture into the K-shell the effect is less distinct than for capture into the L-shell. In any case $\lambda_{\mathrm{NEEC}+n}$ rates are one order of magnitude larger than the corresponding $\lambda_{\mathrm{NEEC}+\gamma}$ value. This is a consequence of the difference in the underlying neutron and gamma-decay cross sections (confer Tab. 5.4).

Without NEEC the gamma-decay rate is found to be two orders of magnitude larger than the neutron emission rate. Upon inclusion of NEEC this ratio is reversed. For capture into L-shell the net neutron decay rate is enhanced by 3 orders of magnitude, while the net gamma-decay rate stays of the same order of magnitude as before. This indicates a strong influence NEEC may have on stellar nucleosynthesis reactions.

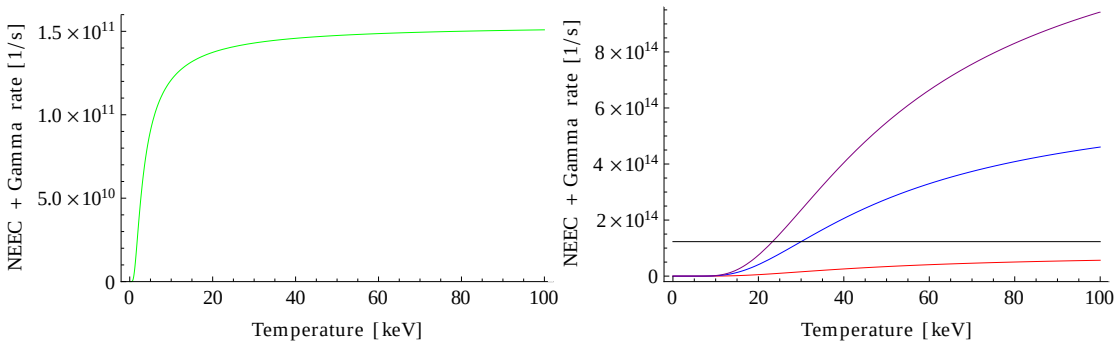

(a) Built-up of $\lambda_{\mathrm{NEEC}+\gamma}$ for K-shell capture.

(b) Built-up of $\lambda_{\mathrm{NEEC}+\gamma}$ for L-shell capture.

Figure 5.1: Combined rates of NEEC and gamma-decay (coloured lines) in comparison to the gamma decay rate of the compound state after neutron capture (black line) as a function of temperature. The K-shell sublevel considered in (a) is $1s_{1/2}$, the L-shell sublevels in (b) are $2s_{1/2} \rightarrow$ red, $2p_{1/2} \rightarrow$ blue $2p_{3/2} \rightarrow$ purple Note the different scaling of the depicted rates.

The temperature dependency of the decay rates can also be investigated. For exemplification we preent all rates leading to gamma-decay of the nucleus in Fig. 5.1. The the photon strength function model and nuclear transition of 90 keV were chosen. The sole gamma-decay rate is independent of temperature in our approximation, while the combined rates $\lambda_{\mathrm{NEEC}+\gamma}$ incorporate a temperature dependent flux and thus vary with temperature themselves. This reveals that the decay rates incorporating NEEC increasingly compete with the sole decay of same type with increasing temperature. Again the effect is stronger for capture into the L-shell.

The interplay of the reaction rates calculated here will be subject of the next section.

5.3 Solution of Network of Rate Equations

The population and depopulation of a system's states can be expressed via the corresponding excitation and decay. The development of the system with time is governed by a set of ordinary linear differential equations of first order. The set of rate equations encompassing neutron capture, neutron emission, gamma decay, NEEC followed by gamma decay and NEEC followed by neutron emission were discussed in section 4.7 and are given in Equations (4.22). In accordance to the introduced transitions governing the neutron capture part of nucleosynthesis of heavy elements, the considered process operates between three levels, in the following called N_1, N_2 and N_3. They represent the initial isotope, the compound state as an excited state of the consecutive isotope and this new isotope in its ground state respectively.

Production into the initial state N_1 and beta-deacy from the final state N_3 are not considered. Therefore only the initial time evolution of the system can be meaningfully considered here. In this regime the occupation of N_1 can be assumed to be constant as the shift of occupation towards N_3 is then only a minor perturbation.

The states N_2 and N_3 are assumed to be completely unoccupied at the beginning, while the pool of atoms available in the system is situated in N_3. The total number of atoms in the system is arbitrarily chosen to be 10^{20}. However, this number is of no imminent importance for our qualitative results.

In Fig. 5.2 we present the resulting occupation of N_3 as a function of time. For both investigated NEEC transition energies, the occupation of N_3 is compared to the reference case of no NEEC happening. Clearly, NEEC quenches the formation of the new isotope for electron capture into the L-shell. For capture into K-shell the effect is much less pronounced and the occupation of N_3 follows closely the same curve as it does without NEEC.

The transition energy of NEEC enters our calculation in the expression of $\lambda_{\mathrm{NEEC}+\beta}$ given in

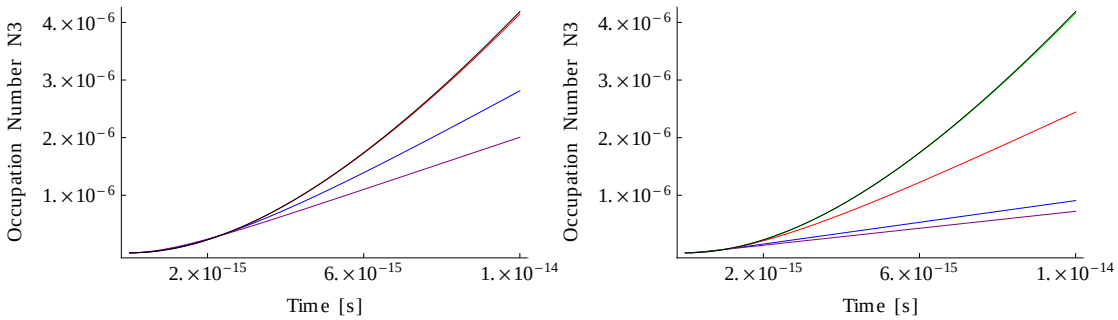

(a) NEEC with 30 keV transition energy **(b)** NEEC with 90 keV transition energy

Figure 5.2: Time evolution of N_3. Black depicts the solution without NEEC, while the coloured graphs show the solution taking NEEC into account for capture into several orbitals. The electron capture occurs in the following atomic levels: $1s_{1/2} \rightarrow$ green, $2s_{1/2} \rightarrow$ red, $2p_{1/2} \rightarrow$ blue, $2p_{3/2} \rightarrow$ purple. The green as well as the red line in (a) and the green line in (b) are covered by the respective black one. This solution is obtained using a B value from the photon strength function.

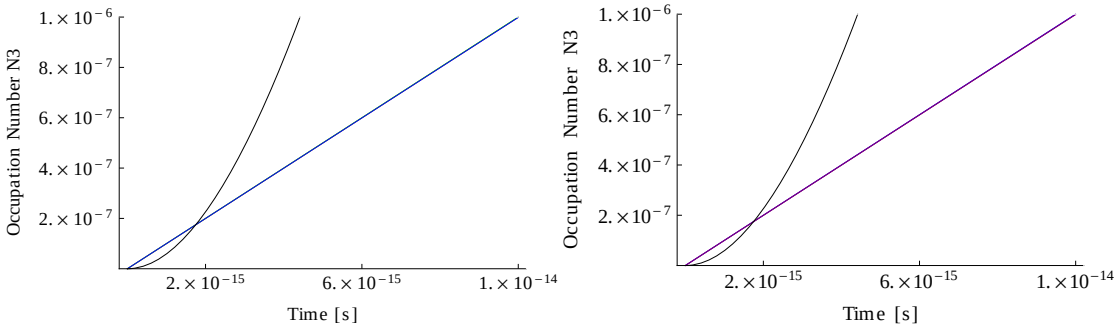

(a) NEEC with 30 keV transition energy **(b)** NEEC with 90 keV transition energy

Figure 5.3: Solution for N_3 of the system of rate equations as presented in (4.22). The graphs of the scenarios including NEEC are colour-coded as follows: $1s_{1/2} \rightarrow$ green, $2s_{1/2} \rightarrow$ red, $2p_{1/2} \rightarrow$ blue, $2p_{3/2} \rightarrow$ purple, which ly nearly on top of one another. The black line depicts the scenario without NEEC. For these plots a B-value derived from sum rules was used. The impact of NEEC is then more pronounced than in Fig. 5.2.

Eq. (5.6). There we have the competing influence of the factors $1/p^2$, Γ_{NEEC} and $\phi(E_{\mathrm{cont}})$. As is apparent from the numerical results tabulated in Tab. 5.6 and 5.5 as well as the plots in Fig. 5.2, NEEC is more effective for the transition energy of 90 keV compared to 30 keV. Apparently the effects of the NEEC transition rate Γ_{NEEC}, which is larger for the 90 keV transition, and the electron flux outweigh the influence of $1/p^2$ in the considered energy regime.

To draw the comparison to the alternative model for B relying on a sum rule we present the corresponding results in Fig. 5.3. Again the increase in occupation of N_3 is found to be decelerated by NEEC with the same dependency on nuclear transition energy as before. In contrary to the previous situation, capture into $1s$ has an equal effect as does capture into an L-shell orbital. Additionally the spread between the outcome for capture into the different atomic states is largely diminished. This is caused by the greater estimate of B applied in these calculations, which substantially enhances the NEEC rate.

The behaviour of the N_3-state occupation was investigated for different temperatures and is depicted in Fig. 5.4. Electron capture into the $2p_{3/2}$ atomic level was chosen as the effects are most pronounced. The occupation increase turns out to be inverse proportional to temperature. This can be explained by the Fermi-Dirac statistics underlying the electron distribution, which is

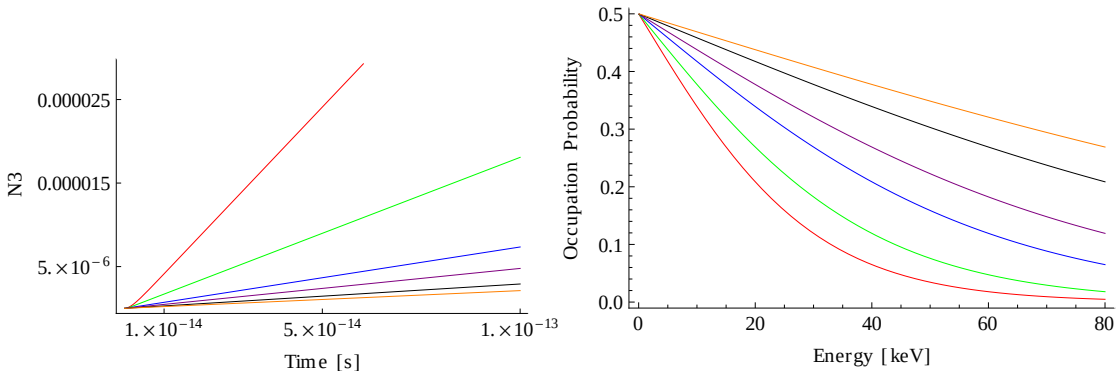

(a) Built-up of occupation of N_3 **(b)** FD distribution for various temperatures.

Figure 5.4: (a) The built-up of the N_3-state occupation as a function of time for various temperatures considering electron capture into the $2p_{3/2}$ shell. Temperatures investigated are $T = 15$ keV $\rightarrow$ red, $T = 20$ keV $\rightarrow$ green, $T = 30$ keV $\rightarrow$ blue, $T = 40$ keV $\rightarrow$ purple, $T = 60$ keV $\rightarrow$ black, $T = 80$ keV $\rightarrow$ orange. (b) The Fermi-Dirac distribution for the same temperatures.

depicted in Fig. 5.4b for the same temperatures as used in Fig. 5.4a and is found to increase with increasing temperature. Thus more electrons are available and the NEEC rate increases. The net neutron emission rates are raised more than the gamma-decay rates and N_3 is less populated.

The magnitude of the net effect of NEEC can be evaluated by investigating the ratio of the occupation of the N_3 state for results including NEEC and not including NEEC at an arbitrary time step

$$R = \frac{N_3^{\text{NEEC}}}{N_3^{\text{no NEEC}}}. \tag{5.7}$$

The obtained result for a choice of two times is presented in Fig. 5.5 for the same case as was studied in Fig. 5.4.

The curve shows a sharp decrease of the occupation ratio with temperature till ≈ 30 keV while for higher temperatures the decrease happens much slower and aligns to a value between 0.05 and 0.2. The curves obtained for the two times 10^{-14} and 10^{-12} differ by a factor of about 2.

This value can be taken as a first estimate of a stellar mitigation factor in the style of the stellar enhancement factor used to give the magnitude of the impact of the occupation of low-lying nuclear levels in stellar scenarios on nuclear processes in these environments. The approximation steps taken are rather rough, and the estimate obtained for the factor by which the occupation of N_3 is quenched should only be taken as an illustrative figure. Additionally we investigated a scenario where the nuclear transition induced by NEEC is expected to have the greatest impact. Accordingly, the order of magnitude of the stellar mitigation factor R introduced here may serve only as an estimation of a lower bound. A calculation of R incorporating the full range of the neutron and electron spectra could as well be much closer to unity.

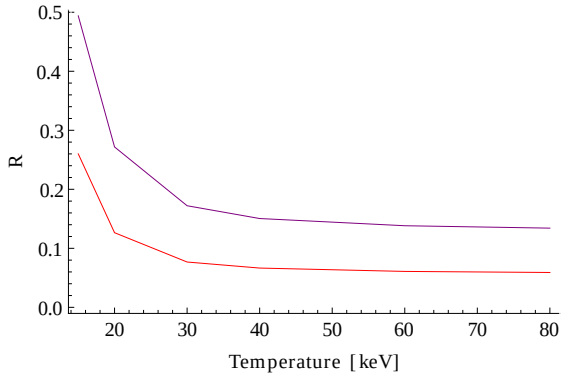

Figure 5.5: Ratio of occupation probability of N_3 with NEEC being included versus rate equations without NEEC, as defined in Eq (5.7), as a function of stellar temperature at the time step $t = 10^{-14}$ s (purple) and $t = 10^{-12}$ s (red). In the case of NEEC being included, capture into the $2p_{3/2}$ orbital is considered.

Summary and Outlook

Summary

In this thesis we have theoretically investigated the role that NEEC can play in nucleosynthesis scenarios of heavy isotopes. In particular, we were interested in the modifications induced by the coupling of the atomic shell to the nucleus on neutron capture reactions in stellar environments. The considered scenario places the NEEC step immediately after neutron capture by the mother nucleus, allowing NEEC to compete with the decay of the newly produced daughter nucleus from the highly excited state close to the neutron emission threshold to the ground state. Due to different decay branching ratios of the excited states before and after NEEC, the latter can modify the production rate of the daughter isotope.

Starting from very basic premises, an estimate was made on the magnitude of the NEEC effect on the production of the daughter isotope. To this end, we chose ^{187}Os as a test case, since the neutron capture properties of this isotope under stellar conditions are required to be known with high accuracy in the Re/Os clock determining the age of the universe. Taking into account nuclear parameters of ^{187}Os, we designed a simple model to incorporate NEEC from the original compound nuclear state together with the other established decay modes to form a combined reaction rate.

The NEEC rate was obtained using the formalism developed by Pálffy [PSH06] for electron capture into the K and L-shells. As a first approximation, the interaction of the plasma with the atomic shell, which would cause shifts to the atomic orbitals, was disregarded. Furthermore, the ionization degree was not investigated and, while the free neutrons and electrons have a broad energy distribution, only specific energy states of the electron and neutron were incorporated into our discussion.

For the nuclear transition contribution in the NEEC rate, the knowledge of the reduced transition probability is required. Due to the lack of either measured values for the reduced transition probability of the nucleus in the continuum spectrum or a previously tested theoretical estimate, we have used two different approximations, one of them involving the photon strength function and the other being suggested in Ref. [BW63]. Both of these approximations can only be taken to be very rough and may be off by several orders of magnitude. The reduced nuclear transition probabilities obtained via the two methods were found to differ by at least four orders of magnitude, a result which emphasizes the caution required in handling these estimates.

Using the more pessimistic choice for the reduced transition probability, we have found that the modified ratio of the gamma-decay rate (leading to the daughter isotope ground state) to the neutron emission rate (leading back to the mother nucleus) caused by the additional NEEC transition reduces substantially the formation of the daughter isotope. Thus, the daughter isotope formation ratio with and without occurrence of NEEC ranges between 0.5 and 0.1 in our model, considering only specific transition energies and electron recombination states. Furthermore, this ratio was found to decrease with temperature in the considered temperature interval of 15 to 80 keV, which can be attributed to an increase in electron flux with temperature. These findings, although at this stage based on several approximations, motivate further studies of the impact of NEEC on nucleosynthesis scenarios.

Outlook

The present approach, due to its approximations, offers many possibilities for extensions and continued consolidations. So far we have focussed on a rather simplified model to estimate the scale of possible effects and to assemble and test models yielding the required parameters such as level density, photon strength, reduced transition probability or the neutron and electron flux. The main unknown remains the nuclear reduced transition probability, where several orders of magnitude uncertainty occur. One first issue to be treated is therefore to find a better estimate and insight into the error introduced by such an estimate.

Despite these large uncertainties, our calculations revealed that NEEC poses a considerable potential for modifying the neutron capture and neutron scattering reaction rates giving thus impetus to additionally extend our model and treat effects so far neglected.

One main direction of interest would be the treatment of plasma effects to better adopt our discussions to the stellar environment. The plasma can induce notable shifts to the electron orbitals. Furthermore, the plasma-energy-dependent ionization degree of atoms in stellar plasmas was not taken into account so far. We merely expected the shells into which electrons are captured to be empty. An approach to this issue is given by the Saha equation [Sah21]. While we have considered only electron capture to occur into the lowest free orbital, in a more general treatment this would be replaced be a formalism where electrons can also be captured into higher states that subsequently decay by photon emission [PHK$^+$08].

Another field of further studies is the extension of our model to the full energy distribution of neutrons and electrons. This would render a theoretical effective (n, γ) neutron capture cross section incorporating NEEC in high-energy plasmas. Similar to the calculation of the stellar enhancement factor, this would yield an appropriate measure to the mitigation of neutron capture by NEEC. Such a general formalism could then subsequently be applied to all isotopes of interest, allowing eventually the tabulation of a stellar mitigation factor for each isotope as is done for the stellar enhancement considerations.

With a more reliable formalism for including the impact of NEEC in astrophysical nucleosynthesis processes, a number of interesting cases can be treated, starting with the full treatment of the Re/Os clock. The branching points at ^{185}W and ^{186}Re also need to be investigated for a correct estimate of the galactic age. Additionally the neutron capture cross section of ^{186}Os corrected for stellar effects is required. Together with ^{187}Os, the cross sections of these four isotopes corrected to include the effect of NEEC would allow to estimate the correction to the galactic age previously calculated.

Bibliography

[ATY84] M. Arnould, K. Takahashi, and K. Yokoi. On the validity of the local approximation for the s-process in the OS region, and implications for the (R-187)-(Os-187) cosmochronology. *Astron. Astrophys.*, 137:51–57, August 1984.

[BBB$^+$] L. A. Bernstein, D.L. Bleuel, C.R. Brune, R.D. Hoffman, I.Y. Lee, L. Phair, and D.H.G. Schneider. Interactions between highly excited nuclei and photons in astrophysical plasmas. unpublished.

[BBFH57] E. Margaret Burbidge, G. R. Burbidge, William A. Fowler, and F. Hoyle. Synthesis of the elements in stars. *Rev. Mod. Phys.*, 29:547–650, Oct 1957.

[BBK$^+$00] Z.Y. Bao, H. Beer, F. Käppeler, F. Voss, K. Wisshak, and T. Rauscher. Neutron cross sections for nucleosynthesis studies. *Atomic Data and Nuclear Data Tables*, 76(1):70 – 154, 2000.

[BCCK92] F. Bečvář, P. Cejnar, R. E. Chrien, and J. Kopecký. Test of photon strength functions by a method of two-step cascades. *Phys. Rev. C*, 46:1276–1287, Oct 1992.

[Bec09] F. Becvar. Photon strength functions of heavy nuclei: Achievements and open problems. *AIP Conference Proceedings*, 1109(1):27–37, 2009.

[BFF$^+$96] F. Bosch, T. Faestermann, J. Friese, F. Heine, P. Kienle, E. Wefers, K. Zeitelhack, K. Beckert, B. Franzke, O. Klepper, et al. Observation of bound-state β^- decay of fully ionized ^{187}Re: ^{187}Re-^{187}Os cosmochronometry. *Phys. Rev. Lett.*, 77:5190–5193, 1996.

[Bri55] D. M. Brink. PhD thesis, Oxford University, 1955.

[BW63] J. M. Blatt and V. F. Weisskopf. *Theoretical Nucelar Physics*. John Wiley & Sons, New York, London, 1963.

[CHA$^+$00] T. Carreyre, M. R. Harston, M. Aiche, F. Bourgine, J. F. Chemin, G. Claverie, J. P. Goudour, J. N. Scheurer, F. Attallah, G. Bogaert, et al. First direct proof of internal conversion between bound states. *Phys. Rev. C*, 62:024311, Jul 2000.

[Cla64] D. D. Clayton. Cosmoradiogenic Chronologies of Nucleosynthesis. *Astrophys. J.*, 139:637–+, February 1964.

[Dau06] D. Dauvergne. Habilitation dissertation, Université Lyon 1, 2006.

[EB05] T. Egidy and D. Bucurescu. Systematics of nuclear level density parameters. *Phys. Rev. C*, 72:044311, Oct 2005.

[EM95] J. Eichler and W. E. Meyerhof. *Relativistic atomic collisions*. Academic Press, San Diego, Calif. [u.a.], 1995.

[FMM$^+$10] K. Fujii, M. Mosconi, A. Mengoni, C. Domingo-Pardo, F. Käppeler, U. Abbondanno, G. Aerts, H. Álvarez-Pol, F. Alvarez-Velarde, S. Andriamonje, et al. Neutron physics of the Re/Os clock. III. Resonance analyses and stellar (n,γ) cross sections of ^{186,187,188}Os. *Phys. Rev. C*, 82:015804, Jul 2010.

[GM96] W. Greiner and J. Maruhn. *Nuclear models*. Springer, Berlin ; Heidelberg [u.a.], 1996.

[GM04] G. Gosselin and P. Morel. Enhanced nuclear level decay in hot dense plasmas. *Phys. Rev. C*, 70:064603, Dec 2004.

[GMM07] G. Gosselin, V. Méot, and P. Morel. Modified nuclear level lifetime in hot dense plasmas. *Phys. Rev. C*, 76:044611, Oct 2007.

[GMM10] G. Gosselin, P. Morel, and P. Mohr. Modification of nuclear transitions in stellar plasma by electronic processes: K isomers in ^{176}Lu and ^{180}Ta under s-process conditions. *Phys. Rev. C*, 81:055808, May 2010.

[GN76] V.I. Goldanskii and V.A. Namiot. On the excitation of isomeric nuclear levels by laser radiation through inverse internal electron conversion. *Physics Letters B*, 62(4):393 – 394, 1976.

[gsi89] Exciting the nucleus by electron capture in axial channeling. Proposal s003, GSI, Darmstadt, 1989.

[Jac62] J. D. Jackson. *Classical Electrodynamics*. J. Wiley, New York, 1962.

[JS85] W.R. Johnson and Gerhard Soff. The lamb shift in hydrogen-like atoms, $1 \leq z \leq 110$. *Atomic Data and Nuclear Data Tables*, 33(3):405 – 446, 1985.

[KBW89] F Käppeler, H Beer, and K Wisshak. s-process nucleosynthesis-nuclear physics and the classical model. *Reports on Progress in Physics*, 52(8):945, 1989.

[KGBA11] F. Käppeler, R. Gallino, S. Bisterzo, and Wako Aoki. The s process: Nuclear physics, stellar models, and observations. *Rev. Mod. Phys.*, 83:157–193, Apr 2011.

[KJBR91] F. Kp̈peler, S. Jaag, Z. Y. Bao, and G. Reffo. The s-process branchings at ^{185}W and ^{186}186. *Astrophys. J.*, 366:605–616, 1991.

[KYS+00] S. Kishimoto, Y. Yoda, M. Seto, Y. Kobayashi, S. Kitao, R. Haruki, T. Kawauchi, K. Fukutani, and T. Okano. Observation of nuclear excitation by electron transition in ^{197}Au with synchrotron x rays and an avalanche photodiode. *Phys. Rev. Lett.*, 85:1831–1834, Aug 2000.

[Lab11a] National Nuclear Data Center Brookhaven National Laboratory. Chart of nuclides, Oct 2011.

[Lab11b] National Nuclear Data Center Brookhaven National Laboratory. Sigma 3.2 - evaluated nuclear data file (ENDF) retrieval & plotting, Oct 2011.

[MB42] H S W Massey and D R Bates. The properties of neutral and ionized atomic oxygen and their influence on the upper atmosphere. *Reports on Progress in Physics*, 9(1):62, 1942.

[MDH81] S. F. Mughabgab, M. Divadeenam, and N. Holden. *Neutron Cross Sections*. Academic Press, New York, London, 1981.

[Mer98] E. Merzbacher. *Quantum Mechanics*. John Wiley and Sons, 1998.

[MFM+10] M. Mosconi, K. Fujii, A. Mengoni, C. Domingo-Pardo, F. Käppeler, U. Abbondanno, G. Aerts, H. Álvarez-Pol, F. Alvarez-Velarde, S. Andriamonje, et al. Neutron physics of the Re/Os clock. I. Measurement of the (n,γ) cross sections of ^{186,187,188}Os at the CERN n_TOF facility. *Phys. Rev. C*, 82:015802, Jul 2010.

[MMG+10] P. Morel, V. Méot, G. Gosselin, G. Faussurier, and C. Blancard. Calculations of nuclear excitation by electron capture (NEET) in nonlocal thermodynamic equilibrium plasmas. *Phys. Rev. C*, 81:034609, Mar 2010.

[PÓ6] A. Pálffy. *Theory of nuclear excitation by electron capture for heavy ions.* PhD thesis, Universität Gießen, 2006.

[PB11] R. K. Pathria and P. D. Beale. *Statistical Mechanics.* Academic Press, 2011.

[PEK07] A. Pálffy, J. Evers, and C. H. Keitel. Isomer triggering via nuclear excitation by electron capture. *Phys. Rev. Lett.*, 99(17):172502, Oct 2007.

[PFG96] F.A. Parpia, C.Froese Fischer, and I.P. Grant. Grasp92: A package for large-scale relativistic atomic structure calculations. *Computer Physics Communications*, 94(2-3):249 – 271, 1996.

[PHK+08] A. Pálffy, Z. Harman, C. Kozhuharov, C. Brandau, C. H. Keitel, W. Scheid, and T. Stöhlker. Nuclear excitation by electron capture followed by fast x-ray emission. *Physics Letters B*, 661(4):330 – 334, 2008.

[PSH06] A. Pálffy, W. Scheid, and Z. Harman. Theory of nuclear excitation by electron capture for heavy ions. *Phys. Rev. A*, 73(1):012715, Jan 2006.

[Pá10] A. Pálffy. Nuclear effects in atomic transitions. *Contemporary Physics*, 51(6):471–496, 2010.

[RS80] P. Ring and P. Schuck. *The Nuclear Many-Body Problem.* Springer, New York [u.a.], 1980.

[RT00] T. Rauscher and F.-K. Thielemann. Astrophysical reaction rates from statistical model calculations. *Atomic Data and Nuclear Data Tables*, 75(1-2):1 – 351, 2000.

[Sah21] M. N. Saha. On a Physical Theory of Stellar Spectra. *Royal Society of London Proceedings Series A*, 99:135–153, May 1921.

[SIN+11] K. Shibata, O. Iwamoto, T. Nakagawa, N. Iwamoto, A. Ichihara, S. Kunieda, S. Chiba, K. Furutaka, N. Otuka, T. Ohsawa, et al. Jendl-4.0: A new library for nuclear science and engineering. *Journal of Nuclear Science and Technology*, 48(1):1–30, 2011.

[SS67] S. Shastry and A.K. Saha. On the collective octupole state of 88sr. *Nuclear Physics A*, 97(3):567 – 571, 1967.

[SUM+05] T. Shizuma, H. Utsunomiya, P. Mohr, T. Hayakawa, S. Goko, A. Makinaga, H. Akimune, T. Yamagata, M. Ohta, H. Ohgaki, et al. Photodisintegration cross section measurements on ^{186}W, ^{187}Re, and ^{188}Os: Implications for the re-os cosmochronology. *Phys. Rev. C*, 72:025808, 2005.

[Tak98] K. Takahashi. The [sup 187]re - [sup 187]os cosmochronometry—the latest developments. *AIP Conference Proceedings*, 425(1):616–625, 1998.

[Tri75] V. Trimble. The origin and abundances of the chemical elements. *Rev. Mod. Phys.*, 47:877–976, Oct 1975.

[WIP+97] G. Wallerstein, I. Iben, P. Parker, A. M. Boesgaard, G. M. Hale, A. E. Champagne, C. A. Barnes, F. Käppeler, V. V. Smith, R. D. Hoffman, et al. Synthesis of the elements in stars: forty years of progress. *Rev. Mod. Phys.*, 69:995–1084, Oct 1997.

[Zim92] P. Zimmerer. *Relativistische Theorie für die Dielektronische Rekombination bei sehr schweren hochgeladenen Ionen.* Dissertation, Gießen, 1992.

Acknowledgements

It is my privilege to give special thanks here to all the people who have contributed in a multitude of ways to this work.

First and foremost I am deeply indebted to Dr. Adriana Pálffy for proposing this inspiring and demanding topic as well as lending her full experience and knowledge to this work. Adriana has been an extremely caring, helpful mentor in the entire course of our collaboration.

I am equally grateful to Prof. Christoph Keitel for welcoming me at the MPIK and his theory division as well as supervising my studies together with Adriana.

In the course of the research presented in this thesis, I additionally had the opportunity to discuss various concepts with Prof. Hans Weidenmüller, for which I am very thankful. I also would like to thank my office colleges for various helpful words of advise on programming and other issues. Thereby they contributed a lot to a thriving collegial atmosphere. For the same reason I also want to give my thanks to the entire division.

Furthermore not unmentioned shall stay the computer administrator Dominik Hertel and the secretary Sibel Babacan of the division, who were always prepared to give help and advise for any computational or administrative issue.

Last but not least I would like to thank Sebastian Isbaner, David Schönleber and again Adriana for their great support and advise in writing this thesis.

Erklärung

Ich versichere, dass ich diese Arbeit selbstständig verfasst und keine anderen als die angegebenen Quellen und Hilfsmittel benutzt habe.

Heidelberg, den 17.10.2011